Original Paper

Geological Characterization of the Miocene–Pliocene Succession in the Semliki Basin, Uganda: Implications for Hydrocarbon Exploration and Drilling in the East African Rift System

Stephen Mutebi,[1] Souvik Sen ⓘ **,[2,8] Tonny Sserubiri,[3] Arka Rudra,[4] Shib Sankar Ganguli,[5] and Ahmed E. Radwan[6,7]**

The Albertine Graben, an active sedimentary petroliferous basin, has gained global attention as the unexplored areas are recently being targeted for hydrocarbon prospectivity. Here, we present the first detailed geological investigation of the Upper Miocene–Pliocene clastic interval in the southern Lake Albert, part of the Semliki Basin. We employed an integrated approach that includes source rock evaluation, reservoir characterization, pore pressure, and geomechanical evaluation. Thermal maturity analyzed from vitrinite reflectance, spore color index, and Rock–Eval T_{max} indicates that the Lower Kasande–Kakara shales are into the early catagenetic maturity, and the onset of oil window occurs at around 2550 m. With 1.8–2.4% total organic carbon content and dead carbon-free hydrogen index of $\sim$ 600 mg S_2/g TOC, a Type I/II oil-prone source rock was inferred, while the state of the thermal maturity reflects on the relatively low free oil yields associated with a poor oil production index. The quartz arenite reservoirs of the Upper Miocene Kasande–Kakara Formation exhibit excellent petrophysical characteristics and possess pore pressure gradients of 0.17–0.24 psi/ft (1 psi/ft = 22.6206 Mpa/km) in two distinct zones (2040.7–2221.5 m and 2554.7–2730 m) with gross vertical thickness of $\sim$ 206 m. The region belongs to a normal faulting tectonic regime where the vertical stress gradient is 0.91–0.93 psi/ft with a lower bound of minimum horizontal stress gradient interpreted as 0.62 psi/ft. The hydrostatically pressured Miocene shales have higher shear failure gradients and exhibited extensive wellbore failures. The implications of geological characterization in both hydrocarbon exploration and future drilling in the basin are envisaged in this research.

KEY WORDS: Thermal maturity, Source rock characterization, Pore pressure, Miocene reservoir, Albertine Graben.

[1]Department of Geoscience, King Ceasor University, Plot 32 King Ceasor Road, Kampala, Uganda.

[2]Dynasty Building, Geologix Limited, Wing A, Level 4, Andheri Kurla Road, Andheri (E), Mumbai, Maharashtra 400059, India.

[3]Directorate of Petroleum-Uganda, Plot 21, 29 Johnstone Road, Entebbe, Uganda.

[4]Lithospheric Organic Carbon (L.O.C.) Group, Department of Geoscience, Aarhus University, 8000 Aarhus, Denmark.

[5]Marine and Deep Seismics Research Group, CSIR-National Geophysical Research Institute, Uppal Road, Hyderabad Telangana State 500007, India.

[6]Faculty of Geography and Geology, Institute of Geological Sciences, Jagiellonian University, Gronostajowa 3a, 30-387 Kraków, Poland.

[7]Exploration Department, Gulf of Suez Petroleum Company, Cairo, Egypt.

[8]To whom correspondence should be addressed; e-mail: souvikseniitb@gmail.com

INTRODUCTION

Over the past decade, there have been numerous hydrocarbon discoveries in the East African Rift play (Cassie et al., 2015; Cloke et al., 2018). These discoveries centered primarily on the Lake Albert Basin, also well-known as the Albertine Graben (Wei et al., 2017; Xu et al., 2018). This has placed Uganda as a promising destination on the upstream map. As of now, around 1.4 + billion barrels of hydrocarbon in-place have been estimated from 20 separate discoveries in the Albert Rift Graben, mostly from the synrift sediments (Cassie et al., 2015; Cloke et al., 2018). Drilling campaigns since 2006 have delivered promising results from the Waraga, Ngassa, Nzizi, and Kingfisher oilfields, where individual wells delivered 20–25 + m of Miocene–Pliocene pay sands with initial flowrates of 12,000–14,500 bopd[1] (barrel oil per day) (Cassie et al., 2015). More than 52 oil seeps (with the Kibiro, Paraa, and Kibuku seeps being the most prominent) have been identified around the Lake Albert, and of these several are speculated to be from a range of lacustrine to mixed terrestrial–lacustrine source rocks (Cassie et al., 2015). A study on the Bwamba fault kinematics (Ruwenzori Horst, Western Uganda) indicated that there is a hydraulic communication between this fault and the Triassic sediments of the Semliki Basin (Hollinsworth et al., 2018), which may have caused seepage along the fault system. With these promising indicators and initial observations, it was of utmost importance to conduct a thorough source rock analysis to understand the thermal maturation and hydrocarbon generation potential of the basin. Previous studies focused on subsurface sedimentary facies, provenance characterization (Gagnevin et al., 2017; Lukaye et al., 2016; Schneider et al., 2016; Wei et al., 2017; Xu et al., 2018), deformation history, and tectonic evolution (Abeinomugisha & Kasande, 2012; Riad & El Etr, 1985; Simon et al., 2017) of various regions and oilfields from the Albertine Graben. However, the detailed source rock geochemistry, petrophysical properties, overall petroleum system, pore pressure, rock-mechanical properties, and reservoir characterization have not been reported previously, which set the premise of this work.

In this study, we report petroleum geochemical data to deliver insights for future hydrocarbon exploration in the basin. The objectives of the geochemical assessment were: (1) to infer the thermal maturity from vitrinite reflectance (R_o in %), spore color index (SCI) and Rock–Eval T_{max} (°C); (2) to decipher gas composition from chromatography and their possible origin from stable carbon and deuterium isotope analyses; and (3) to evaluate source rock potential (e.g., total organic carbon (TOC), hydrogen index (HI), and bulk kerogen type) from Rock–Eval pyrolysis. Moreover, based on available wireline logs, direct downhole measurements, and regional information, we intended (4) to infer reservoir pore pressure gradients, possible fluid contacts to understand potential reservoir distribution and (5) to perform petrographical and petrophysical assessments to deliver insights into the reservoir quality. A successful exploration and appraisal drilling campaign is required to get insights to an area's hydrocarbon potential and, thus, accurate understanding of subsurface geomechanical behavior is needed to deliver safe and stable wellbore to minimize wellbore complexities and cost overrun. One of the studied exploratory wells experienced mechanical stuck pipe within the Miocene shales, resulting in significant nonproductive time ($\sim$ 30 days) and elevated operational cost. A few studies have been published on the tectonic regime and horizontal stress orientation of the East African Rift System (EARS) (Delvaux & Barth, 2010; Karp et al., 2012; Min & Hou, 2018; Stamps et al., 2008, 2014); however, 1D mechanical earth modeling has yet been constructed in the Semliki Basin. Therefore, we performed well-scale geomechanical modeling to (6) assess in situ stress magnitudes and (7) to address borehole instability issues. The outcomes of this work will guide the planning and execution of future exploratory and appraisal drilling campaigns to unlock the potential of the Semliki Basin.

GEOLOGICAL SETTING OF THE STUDY AREA

The Albertine Graben is a part of the 500-km-long Albertine Rift System (Schneider et al., 2016). The graben is situated in the northern extremity of the western branch of the EARS, which extends to Lake Malawi in the south and covers an extensive length of 2100 km (Xu et al., 2018). The EARS has a complex tectonic architecture due to the systematic linkage of single rift basins by intra-continental

---

[1] 1 bopd = 0.1589 cubic meter per day.

transform faults and their segmentation by transfer and accommodation zones (Koehn et al., 2010; Schneider et al., 2016). Sediments were accumulated in the Albertine Rift over multiple rifting phases from the Middle Miocene, while Archean metamorphic and metasedimentary rocks form the basement. The Albertine rift is characterized by three major phases (Pickford et al., 1993): (1) shallow down wrap formed during 12.5–7 Ma; (2) major faulting at 8 Ma forming the first graben followed by accelerated extension; and (3) exhumation of the Rwenzori block, uplift, and warping of the basement structure. The rifting process has resulted in a 50-km-wide en echelon asymmetrical basin with a faulted escarpment on one side and a flexural wrap or faulted monocline on the other side. The graben straddles the border between Uganda and the Democratic Republic of the Congo, and it contains a major Tertiary depocenter now occupied by the Lake Albert. The basin is a full graben (Karp et al., 2012) bounded by two major NNE–SSW trending boundary fault systems with the Bunia fault to the west and the Toro–Bunyoro and Tonya fault system to the east (Karner et al., 2000; Roberts et al., 2012; Simon et al., 2017). Based on earthquake focal mechanism and GPS-based studies, researchers concluded that the area is presently in a WNW–ESE extensional tectonic regime, extending approximately 1.6–4 mm per year (Calais et al., 2006; Delvaux & Barth, 2010; Morley, 2010; Saria et al., 2014).

The study area lies in the Semliki Basin (also known as Semliki transfer zone or Semliki flats), situated at the southern onshore tip of the Lake Albert (Fig. 1). The deposition in the Albertine Graben started in Early Miocene (Simon et al., 2017). The graben fill is characterized by lacustrine and lacustrine margin siliciclastics. The lake level has fluctuated significantly since the Miocene and thick deposits of lake sediments occurred at considerable distances north and south of the present-day lake shoreline. A regional lithostratigraphic column of the Semliki Basin is presented in Figure 2. Based on the lithological interpretation from drill cuttings and well log correlation, the lithostratigraphy of the study area is established and presented in Table 1. The wells were drilled to the Upper Miocene Kasande–Kakara Formation and they encountered a 3000-m-thick Upper Miocene–Pliocene cyclic sandstone–shale succession. Basement rocks were not encountered in the studied wells up to a depth of 3000 m. Nevertheless, Simon et al. (2017) marked the Miocene–basement unconformity

$(17 \pm 0.8$ Ma) in the Semliki basin at ~ 3250 m from well log-based observations.

METHODS AND WORKFLOW

This work investigated data from three vertical exploratory wells, namely Well-A, -B, and -C, drilled into the Upper Miocene–Pliocene stratigraphy of the Albertine Graben, covering approximately 3000 m of the Tertiary succession. Conventional wireline geophysical logs such as gamma ray, resistivity, sonic, and density along with downhole formation pressure measurements and leak-off tests (LOT) were available and were utilized in this work. Geochemical analysis was performed on canned cutting samples from the Upper Miocene–Pliocene intervals of the drilled wells. The detailed methods are discussed in the following subsections.

Geochemical Analysis

Thermal Maturity Analysis

The thermal maturity evaluation is based primarily on R_o, SCI and Rock–Eval T_{max} (°C) analyses. R_o is an extensively used thermal maturity indicator (Baban & Ahmed, 2014; Dembicki, 2017). In this work, the Leitz Ortholux microscope system was used, which was calibrated using a luco sapphire standard (R_o 0.588%) and glass standard (R_o 1.24%) (Jakeman & Cook, 1978). SCI is based on transmitted light microscopy and it is often used in correlation with R_o to confirm thermal maturity based on the spore color (Barnard et al., 1981; Kibria et al., 2020; Tissot et al., 1987; Yule et al., 1998). Rock–Eval pyrolysis-based index, i.e., T_{max} represents the temperature at maximum hydrocarbon generation during the S_2 cycle (Rudra et al., 2017; Tissot et al., 1987). A range of T_{max} values defines the source rock maturity interval (immature to post-mature) (Dellisanti et al., 2010). In this work, Rock–Eval pyrolysis was performed on the prepared and picked cuttings using a Rock–Eval IV Oil Shows Analyzer (OSA). The working standard (Tertiary Standard) was calibrated against the IFP Secondary Standard 59,355. The quality of the data from OSA was controlled by analyzing a standard reference check sample at every tenth sample position in the sample queue. The results of previously analyzed samples were regarded as satisfactory if the standard check
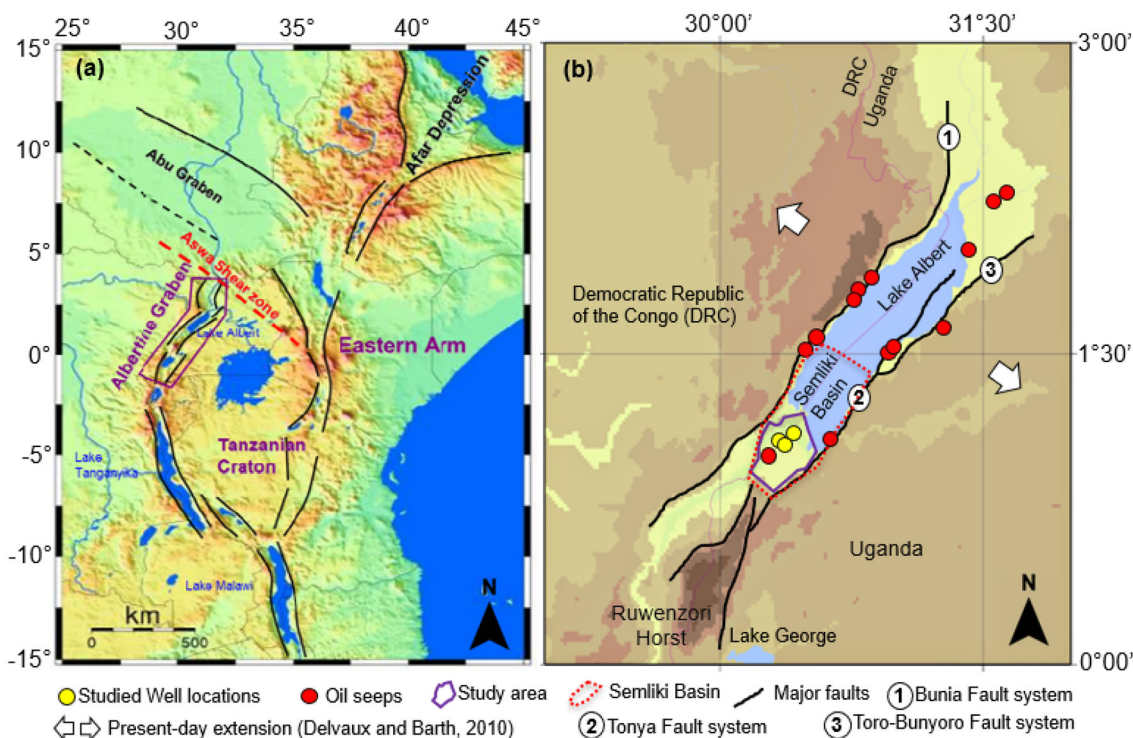
Figure 1. (**a**) Location of the Albertine Graben and Eastern Arm of the East African Rift System (EARS) (Lukaye et al., 2016). (**b**) Detailed map of the Albertine Graben along with the study area, major regional fault system, studied exploratory wells and reported oil seepage locations (Cassie et al., 2015).

values showed tolerance of ± 5% range. Samples suspected to contain anomalous readings for geological reasons were reanalyzed up to a maximum of three times.

Headspace Gas Chromatography Analysis

Headspace gas (C_1–C_5) chromatography analysis was conducted on gases that exsolved out of the cuttings (1200–2500 m) and accumulated in the headspace of canned samples (Waples, 1985). Chromatograms were obtained using a stainless steel column, packed with Chromosorb 102 (80–100 mesh range). The initial column temperature was kept at 160 °C. A flame ionization detector was maintained at 200 °C where ∼ 200 μl of the sample was injected at 200 °C (injector temperature) for 3 min. Helium was used as a carrier gas at flow rate of 100 ml/min at sampling frequency of 2.5 Hz. Quantification of the C_1–C_5 peaks was performed by calibrating the analysis system with a reference gas mixture of known concentrations. This allowed the components to be quantified in terms of concentration given as

parts per million (ppm, or μl/l), from which the normalized % composition of the gas mixture was calculated. The ppm concentrations were converted to microliters of gas per kg of cuttings (μl/kg) by determining the headspace volume and cuttings sample weight. Stable carbon and deuterium isotope analyses were conducted on the methane (CH_4) and carbon dioxide (CO_2) headspace gases of canned samples at selected depths to investigate the likely origin of the methane. Sample selection was based on high concentrations of C_1 and on dry gas mixtures ($C_1 > 99\%$) recorded by C_1–C_5 headspace gas chromatography analyses.

Source Rock Evaluation

Source rock quantity was determined by TOC content and Rock–Eval pyrolysis using the OSA. The quality of the source rock was evaluated based on the Rock–Eval HI, which describes the bulk kerogen type (Types I, II, III, IV), and gross source rock quality (gas-prone versus oil-prone) (Patra et al., 2018), and microscopy analysis of isolated

Age	Formation	Depositional environment
Pliocene	Nyabusosi	Fluctuating coastal to shallow lacustrine
Pliocene- Upper Miocene	Nyakabingo	Repeated prodelatic to delta front progradation
Upper Miocene	Nyaburogo	Delta plain to delta front with switch from humid to semi-arid conditions uppermost
Upper Miocene	Oluka	Lacustine passing into delta plain with minor fluvial intercalations
Upper Miocene	Kakara	Lacustine to delta front to humid delta plain
Upper Miocene	Kasande	Lacustrine to humid coastal mud flat
Middle Miocene	Kisegi	Stacked/amalgamated fluvial sandstones in semi-arid conditions

Figure 2. Regional stratigraphic column of the Semliki Basin (adapted from Lukaye et al., 2016).

Table 1. Lithostratigraphy of the study area, as interpreted from the well logs and drill-cutting information

Start depth (m)	End depth (m)	Series	Formation	Gross lithology
0	200	Pleistocene	Surface Alluvium	Loose sand dominantly, minor traces of soft to moderately hard lignitic material
200	1049	Pliocene–Upper Miocene	Nyabusosi-Nyakabingo	Calystones, interbedded with sandstones and minor siltstones
1049	1500	Upper Miocene	Nyaburogo	Dark gray claystones with sandstones intercalations
1500	1883	Upper Miocene	Oluka	Interbedded claystones, shales, siltstones, and sandstones. Oluka top is marked by dark gray, extremely hard, glassy chert with conchoidal fractures
1883	Well TD	Upper Miocene	Kasande-Kakara	Claystones interbedded with subordinate sands/sandstones

Well TD represents the drilled target depth in the studied wells. Maximum vertical depth of 3000 m is encountered in the Well-B

kerogen in order to identify the various macerals present, assess their state of preservation,, and predict the gross hydrocarbon type likely to be generated at peak maturity. In this work, free oil content (S_1), source potential (S_2) (both in kg/ton unit), oil production index (OPI), HI (mg HC/g TOC), T_{max} (°C), active organic carbon (AOC in wt%), residual organic content (ROC in wt%), and TOC (AOC + ROC; wt%) were measured and interpreted from

Rock–Eval pyrolysis data. Kerogen typing was performed by transmitted white light and fluorescence microscopy for the qualitative and semiquantitative assessment of the different kerogen types and their state of preservation to predict the hydrocarbon types expected at peak maturity. A few kerogen samples were selected for stable carbon isotope analysis ($\delta^{13}C_{kerogen}$).

Reservoir Characterization

Pore Pressure Analysis

A pore pressure (PP) profile was established from available extensive direct pressure measurements using the Compact Repeat Formation tester (MFT) tool, which operates on high precision quartz pressure gauge sensors. These direct formation pressure values provide the most trustworthy estimates (Agbasi et al., 2021; Baouche et al., 2020a; Kassem et al., 2021). Based on MFT values, fluid gradient and hydrocarbon–water contact depths are interpreted in the studied wells. Drilling mud pressures were also applied as PP proxy (Baouche et al., 2021a, 2021b, 2021c; Ganguli et al., 2018; Leila et al., 2021; Radwan, 2021b). The mud pressure was maintained to provide sufficient pressure overbalance to avoid any formation fluid influx.

Reservoir Petrophysical Analysis

Mineral constituents and textural properties of the reservoir sandstones were interpreted from scanning electron microscopic (SEM) analysis of the cutting samples. In the absence of core-based petrophysical measurements, we utilized wireline logs to estimate various reservoir properties (Baouche et al., 2020b). Considering a matrix density of 2.65 g/cc, total porosity was estimated using the bulk-density log. The Archie's equation was applied to infer water and hydrocarbon saturation from the resistivity log with assumed Archie's constant values $a = 1$, $m = n = 1.8$, as suggested for highly porous and permeable sands. Formation water resistivity at in situ temperature was found to be 0.3 Ωm. Based on core measurements, Ongin (2013) established a permeability model for channel sandstones from the nearby EA1 exploration area of the Lake Albert Basin, thus:

$$\text{permeability} = 1.134 e^{23.27 \text{porosity}} \qquad (1)$$

The relationship above was adopted in this study to infer the permeability of the Upper Miocene reservoir sandstones. Based on the shale volume cutoffs, net reservoir thickness is deciphered.

Geomechanical Analysis

In Situ Stress Evaluation

We estimated in situ stress magnitudes from wireline logs and validated them with available downhole measurements. Bulk-density log was utilized to calculate vertical stress (S_v). Because the density log was not recorded in the shallow section, we modeled a synthetic density profile using the Amoco equation, thus (Radwan & Sen, 2021a, 2021b; Radwan et al., 2019, 2020):

$$\text{RHOB}_{\text{Model}} = \text{Rs} + \left(\frac{\text{TVD}}{3125}\right)^{\alpha} \qquad (2)$$

where Rs is sediment density at the surface, TVD stands for true vertical depth, and 'α' is a fitting coefficient. The minimum horizontal stress (S_{hmin}) was estimated by Eaton's method using Poisson's ratio (nu) (Eaton & Eaton, 1997):

$$S_{\text{hmin}} = \frac{v}{1-v}(\text{Sv} - \text{PP}) + \text{PP} \qquad (3)$$

The estimated S_{hmin} was validated with LOT data recorded at the casing shoes. The lower limit of the S_{hmin} was inferred from the frictional faulting mechanism (Zoback, 2007), thus:

$$\frac{S_v - \text{PP}}{S_{\text{hmin}} - \text{PP}} \leq \left[\left(\mu^2 + 1\right)^{0.5} + \mu\right]^2 \qquad (4)$$

where μ is the coefficient of internal friction, which has a default value of 0.6 (Zoback, 2007). The maximum horizontal stress (S_{HMax}) magnitude can be constrained by the extended leak-off test (XLOT) and breakout width from the image logs. These are not recorded in the studied wells and, hence, could not be used. Lang et al. (2011) provided the following relationship to quantify S_{HMax}:

$$S_{\text{HMax}} = S_{\text{hmin}} + k(S_v - S_{\text{hmin}}) \qquad (5)$$

where k is an effective maximum horizontal stress ratio factor. Zhang (2013) suggested $k < 1$ with average value of 0.5 for a normal faulting stress regime. Because the study area is a part of an active rift system, we considered $k = 0.5$ in Eq. 5 to estimate S_{HMax} magnitude from well logs.

Wellbore Stability Analysis

Unstable wellbores are one of the key factors for drilling complexities and associated cost overruns (Abdelghany et al., 2021). Wellbore instability is addressed by the shear failure gradient (SF), which is a measure of downhole fluid pressure that is necessary to prevent the compressive failure of the wellbore wall. SF can be estimated by various rock failure criteria, and the Mohr–Coulomb criterion provides the most conservative estimate (Gholami et al., 2014), thus:

$$\text{SF} = \frac{\{3S_{\text{HMax}} - S_{\text{hmin}} - \text{UCS} + (Q - 1)*\text{PP}\}}{Q + 1} \quad (6)$$

where UCS is unconfined compressive strength; and, Q is from the frictional coefficient, which is calculated as (Gholami et al., 2014):

$$Q = \frac{(1 + \text{Sin}\mu)}{(1 - \text{Sin}\mu)} \quad (7)$$

We analyzed the estimated SF gradient against the formation intervals affected by extensive failures and a lower limit of mud weight is inferred accordingly to ensure a stable wellbore.

RESULTS

Geochemical Characterization and Source Rock Potentiality

Thermal Maturity

The evaluation of thermal maturity is based primarily on R_o and SCI analyses (Fig. 3a and b, respectively) conducted on isolated kerogen recovered from cuttings samples in the interval 620–2470 m belonging to the Pliocene and Upper Miocene. The mean R_o increased from 0.24% at 620 m to 0.47% at 2330 m, which implies that most of the well section analyzed is thermally immature for hydrocarbon generation. Extrapolation of the R_o based maturity profile suggests that the beginning of the oil window (R_o 0.5%) occurred at 2550 m (Fig. 3a). The SCI measurements provided a value of 2 at 620 m, which increased to SCI 4–5/5 at 2330 m (Fig. 3b), combined with the green to greenish lemon-yellow fluorescence characteristics of pollen and spores. The Rock–Eval T_{max} values ranged from 420 to 441 °C, increasing erratically

from approximately 433 °C at 1400 m to 441 °C close to TD (i.e., 2500 m TVD) (Fig. 3c). T_{max} values of > 435 °C suggest that the lower portion of the well section (below 2000 m) has entered the early catagenetic maturity. The R_o and SCI maturity profiles show good agreement (Fig. 3d) and indicate a single maturity gradient. The top of the oil generation window corresponding to R_o 0.5% and SCI 5 occurred at 2400–2550 m near the base of the well section. Extrapolation of the maturity gradients below TD suggests that the generally accepted peak oil generation window corresponding to R_o 0.7% to R_o 1.0% and SCI 6–7 to SCI 8 would extend from 3500 to 4500 m. The logarithmic regression trend fitted through the mean R_o values and the linear regression trend fitted through the SCI values both intersect the surface at zero maturity (R_o 0.20%, SCI 1), indicating that the well section has not experienced significant net uplift and erosion, and it is presently at maximum burial and maturity.

Headspace Gas Evaluation

Gas chromatography analyses were conducted on the C_1–C_5 headspace gases of canned samples over the interval 1200–2487 m. Gas concentrations are presented in Figure 4. Total C_1–C_5 gas concentrations show a broad trend toward lower values with depth. Significantly higher concentrations (mostly C_1) were noted at 1290 m, 1420 m, and 1450 m (samples selected for gas isotope analyses) (Fig. 4). Marginally higher total gas concentrations recorded at 1580–1700 m (Oluka shales), 1940–2100 m (Kakara shales) and below 2440 m (Kasande shales) correspond to the source rock zones that contain kerogen assemblages. These zones are also characterized by slightly significantly higher concentrations of C_2, C_3, iC_4, nC_4, and iC_5. The nC_5 component (pentane) shows a marginally different trend, in which higher concentrations were recorded at 2120–2220 m (Kasande–Kakara shales) (Fig. 4). Gas dryness shows a general trend toward decreasing values with depth from 95% in the Nyaburogo Formation to 40% at the base of the well (Fig. 5). This reflects increase in thermal maturity and subsurface temperature. The iC_4/nC_4 ratio provided a broad maturation trend associated with immature sediments with values decreasing downhole from 3–4 at 1200–1470 m to 0.6–1.4 at 2140–2300 m. Potential source rock zones are highlighted by positive deviations in the iC_4/nC_4 and iC_5/nC_5 ratios,
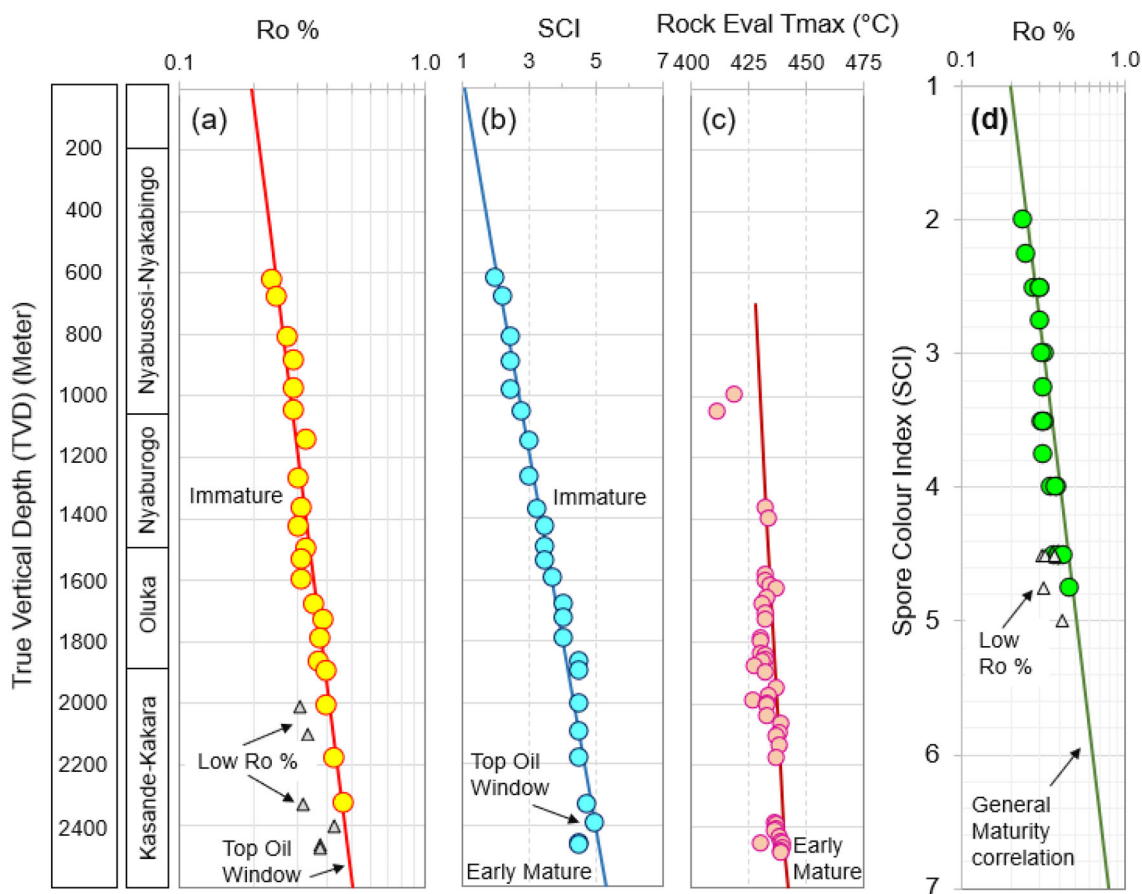
Figure 3. (**a**) Vitrinite reflectance (R_o %) maturity profile. (**b**) Spore color index (SCI) maturity profile. (**c**) Rock–Eval T_{max} maturity profile. (**d**) Correlation of mean R_o % and SCI, and comparison with the correlation scheme. Formation intervals are provided as in-between panels.

and iC_4 and iC_5 concentrations at 1940–2050 m (e.g., organic-rich carbonaceous shales) and 2440–2488 m (oil-prone source rocks) which are associated with fluorescence noted at the well site.

Stable carbon and deuterium isotope analyses were conducted on the methane (CH_4) and carbon dioxide (CO_2) headspace gases of canned samples at 1290 m, 1420 m, and 1450 m to investigate the likely origin of the methane (Table 2). At 1290 m and 1450 m, the $\delta^{13}C_{Methane} > -40‰$ ($-25.47‰$ and $-28.38‰$, respectively), whereas at 1420 m, the $\delta^{13}C_{Methane}$ value was $-42.64‰$. The $\delta D_{Methane}$ value at 1290 m and 1450 m were more than 150‰ ($-139‰$ and $-131‰$, respectively), while the same in the 1420 m sample was $-164‰$. The $\delta^{13}C_{Methane}$ and $\delta D_{Methane}$ values indicated isotopically heavy methane at 1290 m and 1450 m, consistent with a deep post-mature thermogenic dry gas source, but the plausibility of this remains uncertain. The sam-

ple at 1420 m was isotopically lighter in both ^{13}C and ^2H and, for such a case, it more closely resembles a thermogenic oil-associated wet gas source, but this was not supported by the dry composition (99.7% C_1) without invoking compositional fractionation of the gases during migration. A cross-plot between $\delta^{13}C_{Methane}$ and $\delta D_{Methane}$ is presented in Figure 6. The generation of isotopically light methane from the microbial degradation of organic matter during diagenesis is balanced by the generation of isotopically heavy carbon dioxide ($\delta^{13}C_{CO2} > -30‰$). The $\delta^{13}C_{CO2}$ values obtained at 1290 m and 1450 m occurred within these general limits. Interpretation is more complex where methane (bacterial or thermogenic) is oxidized by bacteria to water and isotopically light carbon dioxide ($\delta^{13}C_{CO2} -59‰$ to $-20‰$), so that the remaining methane becomes isotopically heavier and resembles thermogenic methane. The $\delta^{13}C_{CO2}$ values recorded at 1290 m
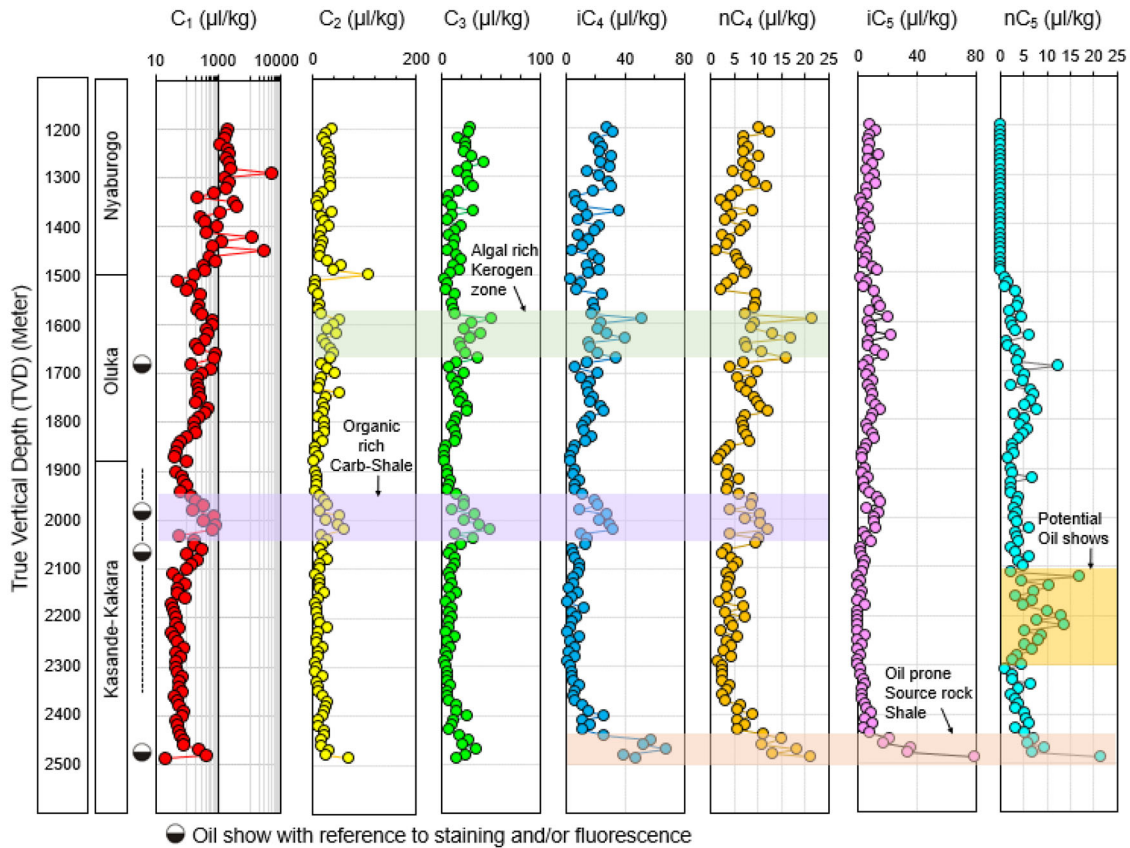
Figure 4. Headspace gas concentration expressed in microliters of gas per kg of rock (μl/kg), measured from the canned samples over the interval 1200–2488 m from the exploratory well.

and 1450 m were well within the range for the bacterial oxidation of methane. The fact that the carbon isotopic composition of both methane and carbon dioxide is almost identical suggests that these two gases were in isotopic equilibrium. It is quite feasible in the case of reduction of CO_2 to CH_4 and the oxidation of CH_4 to CO_2 to have occurred together. These processes would most likely obscure the isotopic characteristics of the original methane gas. Therefore, two alternative interpretations are provided to explain the isotopic composition of the methane and carbon dioxide at 1290 m, 1420 m, and 1450 m: (a) thermogenic oil-associated wet gas origin for the methane at 1420 m, and a thermogenic dry gas origin for the methane at 1290 m and 1450 m; or (b) equilibrium between methane and carbon dioxide due to complementary microbial processes (CH_4 oxidation and CO_2 reduction).

Source Rock Evaluation

Rock–Eval pyrolysis was conducted on washed and dried handpicked cuttings from the 1000–2487 m interval. The results and the data are presented in Figure 7 and Table 3. The majority of samples analyzed in the Oluka, and Kakara–Kasande Formations were organically rich medium/dark gray and olive-gray shales with TOC values in the range of 1–2% with average TOC of about 1.5%. Higher values were recorded in medium gray shales at 1370 m and 1400 m depths (TOC 3.1–3.6%), and dark gray carbonaceous shales at 1990 m, 2010 m, and 2040 m (TOC 5.7–8.0%). The shales encountered at the 2480–2488 m depth range provided TOC values of 1.8–2.4%. AOC represented approximately 10% of the TOC for majority of the samples in the interval of 1400–2000 m, while the remaining 90% was ROC. Not surprisingly, these samples have poor to moderate source
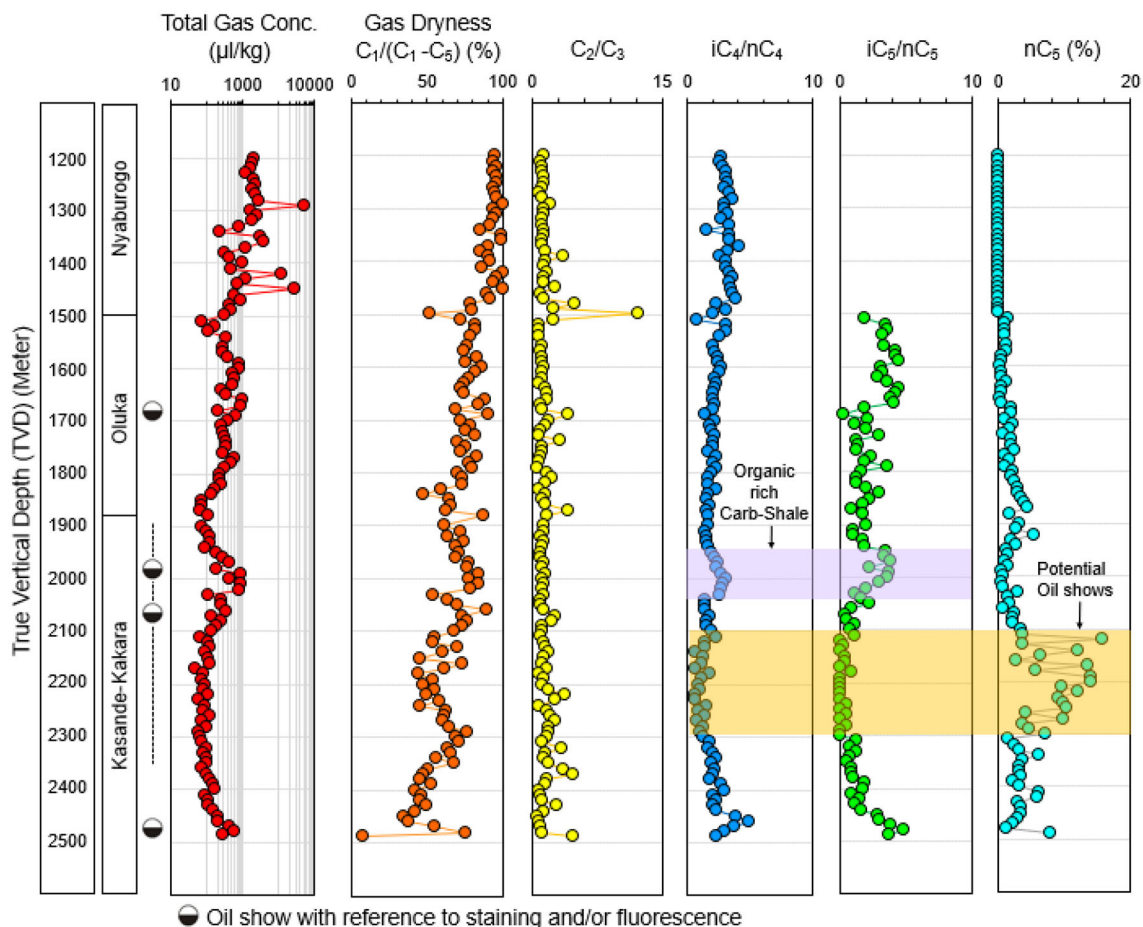
Figure 5. Headspace gas ratio analysis, as measured from the canned samples over the interval 1200–2488 m from the exploratory well.

Table 2. Headspace gas stable isotope results (‰) and generalized interpretation of methane isotope values (‰)

True vertical depth (m)	Gas dryness	$\delta^{13}C_{Methane}$	$\delta D_{Methane}$	$\delta^{13}C_{CO2}$
Gas stable isotope results (‰)				
1290	99.9%	− 25.47	− 139	− 25.55
1420	99.7%	− 42.64	− 164	No data
1450	99.9%	− 28.38	− 131	− 28.3

Maturity stages	Gas dryness	$\delta^{13}C_{Methane}$	$\delta D_{Methane}$	Gas type
Interpretation scheme of methane isotope values (‰)				
Diagenesis—immature	≥ 97%	− 90 to − 55	< − 180	Dry gas
Catagenesis—mature (oil)	< 98%	− 55 to − 30	< − 140	Wet gas
Metagenesis—post-mature	≥ 97%	− 40 to − 20	> − 150	Dry gas

potential to generate hydrocarbons, based on S_2 values of 0.3–3.3 kg/ton (average 1.90 kg/ton). The organically rich carbonaceous shales analyzed at 1990 m, 2010 m and 2040 m had a marginally higher proportion of active organic carbon (14–26% of TOC), which exhibit very good source potential, as
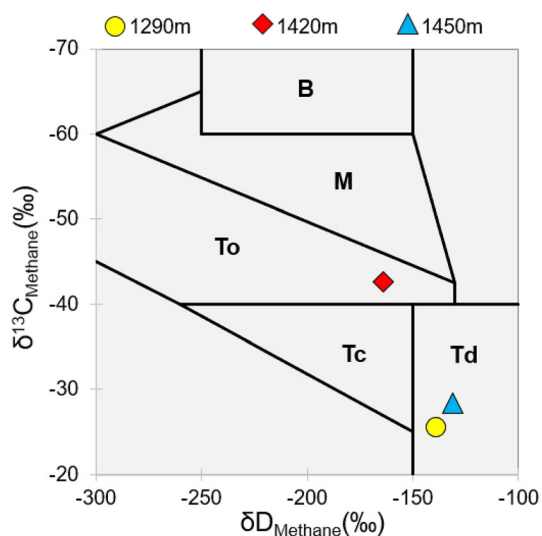
Figure 6. Cross-plot of deuterium ($\delta D_{\text{Methane}}$) and carbon ($\delta^{13}C_{\text{Methane}}$) isotope values for the headspace methane in selected samples (1290 m, 1420 m, and 1450 m). B = bacterial methane, M = mixture of bacterial and thermogenic methane, T = thermogenic methane associated with oil (To), condensate (Tc) and dry gas (Td).

inferred from S_2 values of 12.7–17.9 kg/ton. The highest proportion of AOC was encountered in dark gray shales at 2070–2100 m (AOC 34–42% of TOC) and medium-dark gray shales at 2480–2488 m (AOC 26–34% of TOC). These samples have good source potential with pyrolysate yields in the region of 10 kg/ton. All of the samples analyzed provided relatively low free oil yields (S_1 mostly < 0.2 kg/ton of rock) associated with OPI values of < 0.1. These results reflect relatively low thermal maturity levels in the studied exploratory well and confirm that the oil was indigenous (not migrated) while being in the early stage of oil generation. The higher OPI values of 0.1–0.2 at 1990 m and 2040 m depths are associated with the carbonaceous shales (lower permeability than normal shales). The most prospective oil-prone source rocks are the dark gray shales at 2070–2140 m, 2400 m, and 2470–2488 m. HI values of 283–503 mg S_2/g TOC suggest a Type III–II bulk source rock quality (gas–oil-prone), while the microscopy reveals a mixture of kerogen types: liptinite (non-marine algae, Type I), amorphous organic matter (AOM, Type I or II) and vitrinite (Type III) that range from oil-prone to gas-prone (Fig. 8). Thus, the measured HI values reflect merely the bulk source quality of the organic assemblage as a whole rather than the quality of the individual

kerogen types. In other words, the true quality of oil-prone kerogen was not reflected by the measured HI values due to dilution by gas-prone and inert kerogen. A solution to this problem was given by a plot of TOC versus S_2, from which a dead carbon-free hydrogen index (HI′) can be calculated for the oil-prone fraction (gradient of the regression line). Applying this to the studied exploratory well data yielded HI′ values of approximately 600 mg S_2/g TOC for the oil-prone shales, which indicate a Type I/II good oil-prone source rock quality (Fig. 9).

Reservoir Pore Pressure Distribution

Direct downhole MFT measurements were taken extensively in the Upper Miocene Kasande–Kakara Formation, which offer over 900 m of cyclic sequences of high frequency sandstone–shale intercalations. The overall pressure gradient was close to the fresh water gradient of 0.433 psi/ft^{2} and devoid of any significant over-pressured intervals (Fig. 10a). Based on the MFT gradients, two major hydrocarbon zones were identified and presented in Table 4. Each zone was subdivided into several layers (numbered as A–E alphabetically from shallow to deeper) separated by sealing shales. The MFT data show that at least some of the layers have their own pressure regimes distinct from their neighbors. Overall, the MFT gradient appeared between 0.17 and 0.24 psi/ft. This is consistent with the presence of light hydrocarbons observed from the cutting fluorescence recorded during mud logging. Data from the 1C, 1D, and 1E zones suggest pressure gradients of ∼ 0.17–0.21 psi/ft, consistent with the presence of gas-condensate (Fig. 10b). There was insufficient data from Z1A and Z1B to determine any pressure profiles in these layers, although it was reasonable to assume that these have similar gradients. The intersection of the pressure profile for Z1E and the underlying water, in conjunction with the log data, suggests a hydrocarbon–water contact was located at 2221.5 m MD (measured depth, with ground level as reference datum)/1577.5 m TVDSS (true vertical depth subsea, with mean sea level as reference datum) (Fig. 10b). MFT gradients within the Zone 2 layers varied in the range of 0.19–0.24 psi/ft, which is consistent with the presence of gas-condensate. The intersection of the pressure profile for Z2D and the
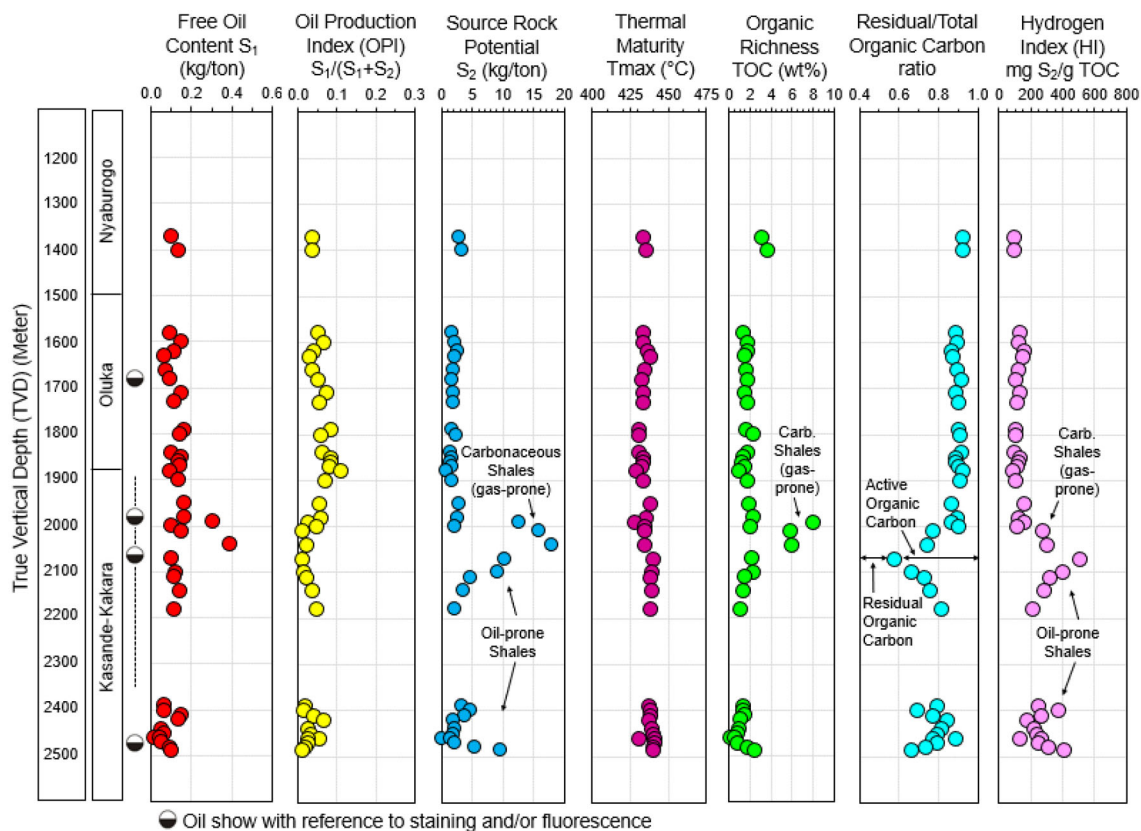
---

[2] 1 psi/ft = 22.6206 MPa/km.

Figure 7. Rock–Eval Pyrolysis data, conducted on the washed and dried handpicked cuttings of the exploratory well.

underlying water suggests a free-water level at 2730 m MD/2078 m TVDSS (Fig. 10c).

Characterization of Reservoir Properties

The Upper Miocene Kasande–Kakara sandstone reservoirs display relatively high resistivity signatures along with the density-neutron porosity crossovers. The SEM analysis indicates that the Upper Miocene reservoirs are composed principally of quartz framework grains with authigenic clays forming the matrix, and calcite cement which binds the quartz grains (Fig. 11a, b). Both grain and matrix-supported textures were observed (Fig. 11c, d). The reservoir is composed primarily of quartz grains (> 90%), with feldspars and lithic fragments representing the rest 10% (Fig. 11). According to the ternary plot, the Upper Miocene Kasande–Kakara sandstone reservoirs can be classified as quartz arenite (Q90 F5 L5). Wireline logs indicate that the individual sandstone intervals had an average

thickness range of 1–10 m, intercalated with shales, forming a high cyclicity clastic sequence. Direct temperature measurements refer to a reservoir thermal gradient of 35 °C/km. The log-based petrophysical evaluation suggests that the Upper Miocene sandstones have excellent reservoir qualities (19–32% porosity and > 150 mD[3] permeability) (Fig. 12). Water saturation in the hydrocarbon-bearing zones was low to moderate in the cleaner, thicker-bedded sands ($\sim$ 30–40%), and commonly moderate to high (50–90%) in the thinner-bedded shaley sands. Average petrophysical parameter values along with the shale volume-based net pay thickness of both the reservoir zones are presented in Table 4. The petrophysical attributes could not be calibrated due to lack of core measurements; however, the fine–medium to coarse–very coarse grain size and weakly consolidated nature of the cleaner sandstone beds imply superior reservoir qualities.

---

[3] 1 mD (millidarcy) = 0.986923 * 10^{-15} m[2.]

Table 3. Rock–Eval Pyrolysis data table from the Well-A

Sample depth m	S_1 kg/ton	S_2 kg/ton	T_{max} °C	OPI	ROC wt%	ROC/TOC	TOC wt%	HI mg S_2/g TOC
1370	0.10	2.82	433	0.0342	2.8976	0.9228	3.14	89.809
1400	0.13	3.34	435	0.0375	3.3020	0.9198	3.59	93.036
1580	0.09	1.68	433	0.0508	1.1431	0.8861	1.29	130.233
1600	0.15	2.09	433	0.0670	1.5541	0.8931	1.74	120.115
1620	0.11	2.62	436	0.0403	1.4734	0.8667	1.7	154.118
1630	0.06	2.18	438	0.0268	1.2741	0.8727	1.46	149.315
1660	0.07	1.87	434	0.0361	1.3690	0.8948	1.53	122.222
1680	0.09	1.66	432	0.0514	1.5148	0.9125	1.66	100.000
1710	0.15	1.90	433	0.0732	1.2899	0.8835	1.46	130.137
1730	0.11	1.96	433	0.0531	1.5182	0.8983	1.69	115.976
1790	0.16	1.76	431	0.0833	1.4906	0.9034	1.65	106.667
1800	0.14	2.31	431	0.0571	2.0367	0.9092	2.24	103.125
1840	0.10	1.56	431	0.0602	1.5722	0.9194	1.71	91.228
1850	0.15	1.68	433	0.0820	1.1681	0.8849	1.32	127.273
1860	0.13	1.41	433	0.0844	1.0322	0.8898	1.16	121.552
1870	0.14	1.63	432	0.0791	1.3231	0.9001	1.47	110.884
1880	0.09	0.74	429	0.1084	0.8211	0.9226	0.89	83.146
1900	0.13	1.74	433	0.0695	1.6048	0.9118	1.76	98.864
1950	0.16	2.85	438	0.0532	1.6002	0.8650	1.85	154.054
1980	0.16	2.69	435	0.0561	2.0235	0.8953	2.26	119.027
1990	0.30	12.73	428	0.0230	6.9085	0.8646	7.99	159.324
2000	0.10	2.12	434	0.0450	1.7457	0.9045	1.93	109.845
2010	0.15	15.83	434	0.0094	4.4137	0.7689	5.74	275.784
2040	0.39	17.88	434	0.0213	4.3636	0.7421	5.88	304.082
2070	0.10	10.41	440	0.0095	1.1977	0.5786	2.07	502.899
2100	0.12	9.21	439	0.0129	1.5356	0.6648	2.31	398.701
2110	0.11	4.71	438	0.0228	1.0899	0.7315	1.49	316.107
2140	0.14	3.62	439	0.0372	0.9679	0.7562	1.28	282.813
2180	0.11	2.17	438	0.0482	0.8408	0.8163	1.03	210.680
2390	0.06	3.22	437	0.0183	1.0578	0.7953	1.33	242.105
2400	0.06	4.83	438	0.0123	0.9041	0.6902	1.31	368.702
2410	0.15	3.68	438	0.0392	1.0921	0.7745	1.41	260.993
2420	0.13	1.88	437	0.0647	0.8932	0.8426	1.06	177.358
2440	0.05	2.13	439	0.0229	0.7891	0.8135	0.97	219.588
2450	0.06	1.87	440	0.0311	0.6198	0.7946	0.78	239.744
2460	0.01	0.17	431	0.0556	0.1151	0.8851	0.13	130.769
2460	0.04	1.48	441	0.0263	0.4338	0.7747	0.56	264.286
2470	0.05	2.05	441	0.0238	0.6557	0.7900	0.83	246.988
2480	0.09	5.53	440	0.0160	1.3135	0.7379	1.78	310.674
2488	0.10	9.62	440	0.0103	1.5632	0.6596	2.37	405.907

S_1 = free oil content, S_2 = source rock potential, OPI = oil production index, ROC = residual organic carbon content, TOC = total organic carbon content, HI = hydrogen index. The dataset is graphically presented in Figure 7

Distribution of In Situ Stresses

Vertical stress was modeled from density logs as the first step of a well log-based geomechanical modeling workflow. Considering a 1.6 g/cc density of surface sediment (Rs), a coefficient (α) value of 0.55 in Eq. 2 provided the best fitting synthetic density profile, which follows the wireline bulk-density log trends nicely in the three exploratory wells (Fig. 13). The S_v gradient was estimated as 0.91–0.93 psi/ft

(Fig. 14a). The following relationship between S_v and vertical burial depth (TVD) was obtained:

$$S_v = 1.3521 \ TVD^{1.0952} \qquad (8)$$

The relationship above can be considered as a regional model and it is advantageous in situations of poor density log quality or data unavailability. The reservoir pore pressure gradient was already discussed in the previous section. Density log-based shale porosities were found to follow a porosity compaction trend line and did not deviate consid-
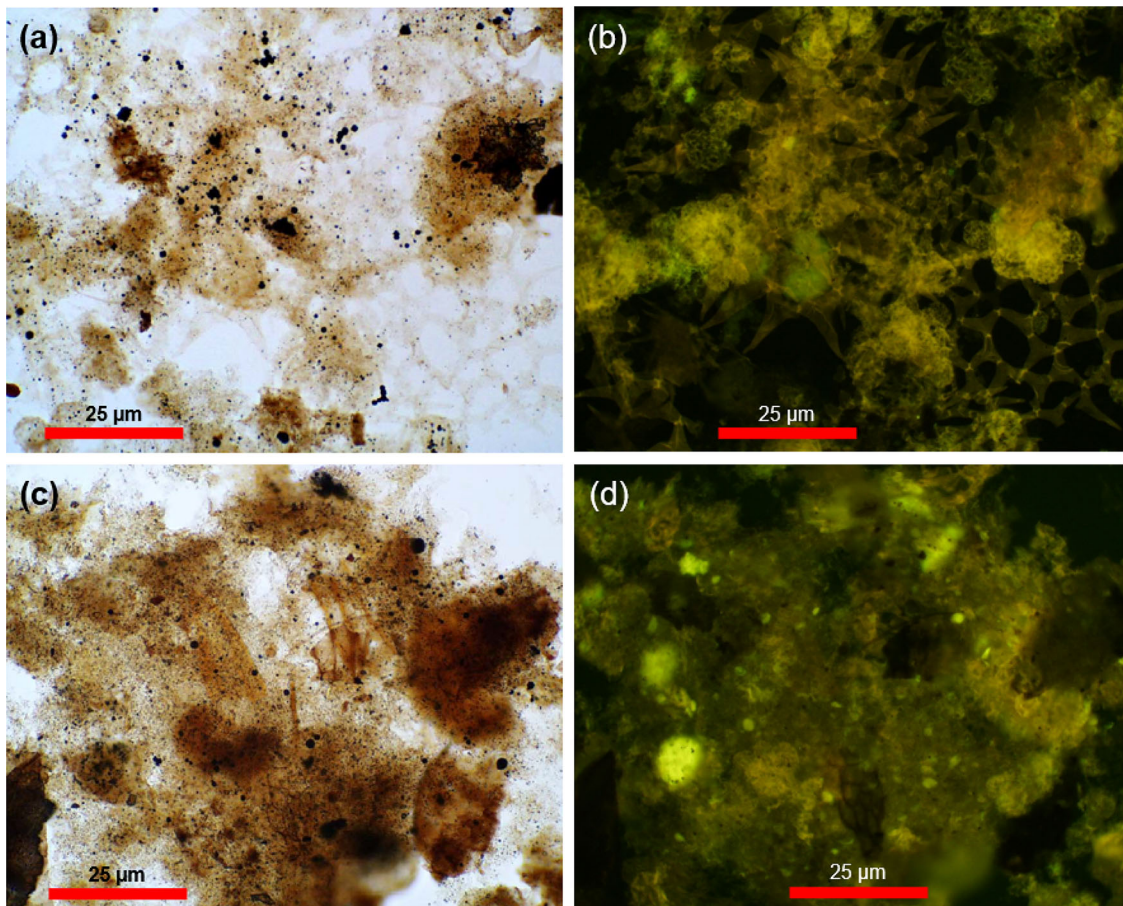
Figure 8. Photomicrographs of various kerogens encountered in the Kasande–Kakara Formations. Algal kerogen (**a**) under transmitted light and (**b**) UV-fluorescence light. The algal matters appear as globular or cog wheel shaped colonies with several lobes. Various structures like circular pits are visible under fluorescence. Amorphous organic matter (AOM) (**c**) under transmitted light and (**d**) UV-fluorescence light. AOM appears as structureless, grayish brown colored with diffused edges with moderate to strong patchy fluorescence.

erably (Fig. 14b), indicating a hydrostatic pore pressure regime. The entire stratigraphy was drilled with a drilling fluid gradient of 0.47 psi/ft. Formation fluid influx or connection gas events were not recorded during drilling. This information indeed indicates that shale pore pressure was less than the applied drilling fluid gradient, and in pressure equilibrium with the reservoir sandstone intervals. An overall fresh water gradient of 0.43–0.44 psi/ft was considered in the entire Upper Miocene to Pliocene sequence in the study area (Fig. 14a). Three LOT and three FIT measurements available from the studied wells indicated a 0.75 psi/ft gradient (Fig. 14a), which can be considered as an upper limit of the S_{hmin} gradient. A more detailed approach was utilized to assess the S_{hmin} profiles from well logs by
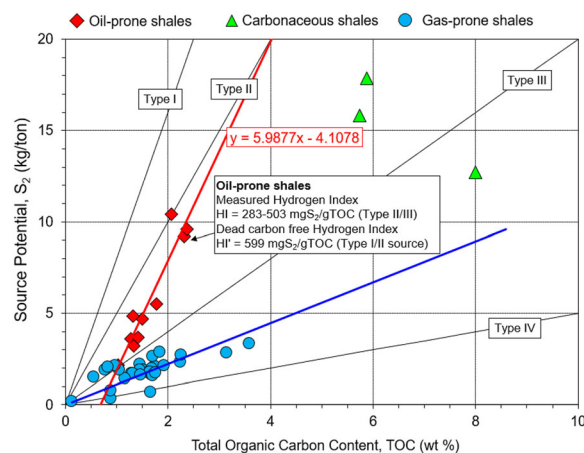

Figure 9. Calculation of Dead Carbon-free Hydrogen Index (HI′) and interpretation of the source rock quality.
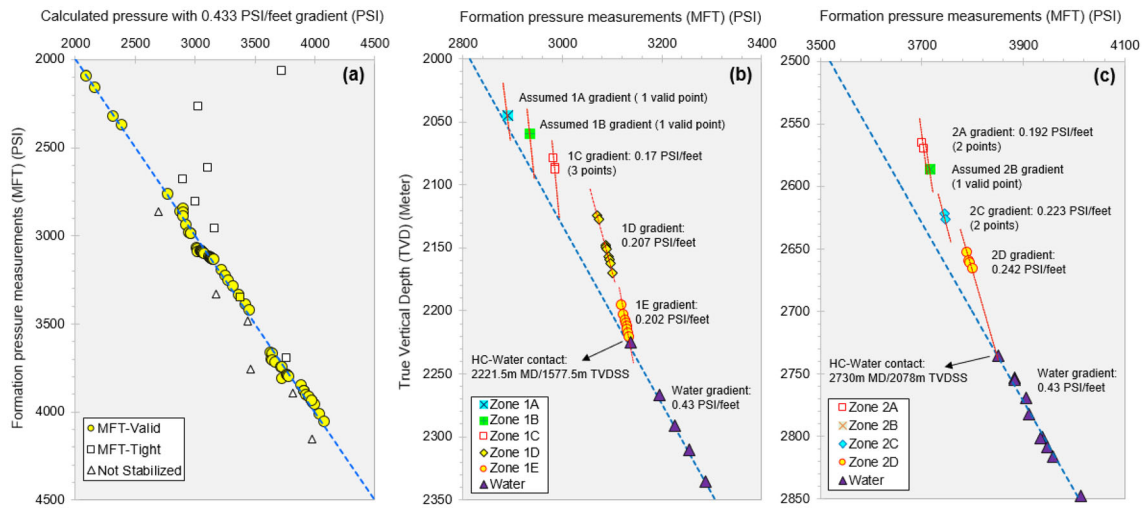
Figure 10. (a) Cross-plot of MFT pressures vs. calculated pressures with fresh water gradient. This indicates that the Upper Miocene sandstones are hydrostatically pressured and devoid of any significant overpressure. (b) and (c) Interpreted hydrocarbon-bearing zones (1 and 2) and layers (A–E) in the Upper Miocene Kasande–Kakara Formation, based on the MFT measurements. Fluid gradients vary between 0.17 and 0.24 psi/ft, indicating light hydrocarbons. Data belong to Well-B.

employing the Poisson's ratio, which is sensitive to lithologies. Sonic log derived Poisson's ratio averaged at 0.24 and 0.34 against the sandstones and shales, respectively (Fig. 15). Shale intervals displayed a 0.74 psi/ft S_{hmin} gradient, similar to the LOT-based values, while the sandstone-dominated sections provided a lower gradient (0.65 psi/ft). The frictional faulting model constrained the S_{hmin} lower limit as 0.62 psi/ft in our study area (Fig. 15). Equation 4 yielded an average S_{HMax} gradient of 0.8 psi/ft (Fig. 15). However, S_{HMax} can effectively range between 0.75 and 0.91 psi/ft (between the upper estimate of S_{hmin} and the lower estimate of S_v). A comprehensive 1D mechanical earth model of the studied interval is presented in Figure 15.

Wellbore Instability and Shear Failure Pressure Analysis

Borehole stability assessment was very critical in the studied Albertine Graben field as one of the wells (Well-A) experienced mechanical stuck pipe at a depth of 2490 m TVD and could not be drilled further. It resulted in a 30-day fishing operation, which is considered as nonproductive times. When studied and correlated with the other exploratory wells, it was found that the drill pipe was stuck within the thick Upper Miocene shale interval

(2450–2560 m TVD). This provided an excellent opportunity to study this interval in detail from Well-B to shed more light on wellbore instabilities to ensure stable wellbore by recommending safe mud weight. The Mohr–Coulomb rock failure model-based results indicated a higher shear failure (SF) pressure gradient in all the Upper Miocene shale intervals (around 9.5–10.2 ppg[4] mud weight equivalent) (Fig. 16), while the sandstones had an SF gradient of about 8.8 ppg (mud weight equivalent). This entire section was drilled using roughly 9 ppg (mud weight equivalent) in all the three wells. Because the mud weight was lighter than the shale SF gradient, it failed under compression. The interpretation was validated with the caliper log-based observations, where selective borehole enlargements were encountered in the shales while the sandstone intervals revealed a gauged hole condition (Fig. 16). A clean shale section in the 2450–2560 m TVD interval was the most vulnerable section of the well in terms of wellbore stability issues. In Well-B, this section showed an average difference of 2″ (= 5.08 cm) between the bit size (4.75″) (= 12.065 cm) and the caliper readings, with a maximum observed hole diameter of 9.9″ (= 25.146 cm) (Fig. 16). With this high degree of caving and borehole wall collapse, hole cleaning became very challenging, and this has led to stuck

---

[4] 1 ppg (pound per gallon) = 1.177 kPa/m.

Table 4. Summary of the log-based petrophysical attributes of the interpreted hydrocarbon-bearing zones and layers in the Upper Miocene Kasande–Kakara Formation

Zone	Layer	True vertical depth (TVD)			Petrophysical properties				
		Top (m)	Base (m)	Gross thickness (m)	Average porosity (%)	Average permeability (mD*)	Average Sw (%)	Net pay with 10% VShale cutoff	Net pay with 20% VShale cutoff
1	A	2040.7	2047	6.3	28	500	75	4.8	5.1
	B	2055	2062.5	7.5	24	280	74	6.1	6.4
	C	2078.5	2089	10.5	23	300	73	4.2	4.7
	D	2115	2171.5	56.5	30	700	54	15.4	19.3
	E	2186	2221.5	35.5	32	900	46	18.2	18.9
Zone 1 gross thickness 116.3 m in TVD, Net pay 48.7 m and 54.3 m based on 10% and 20% VShale cutoff									
2	A	2554.7	2571.5	16.8	23	400	45	9.1	9.8
	B	2581.5	2594	12.5	19	150	73	4.2	5.2
	C	2621	2627.5	6.5	25	350	40	6.1	6.4
	D	2652	2730	78	22	300	73	16.1	19.4
Zone 2 cumulative gross 89.8 m in TVD, Net pay 35.5 m and 40.8 m based on 10% and 20% VShale cutoff									

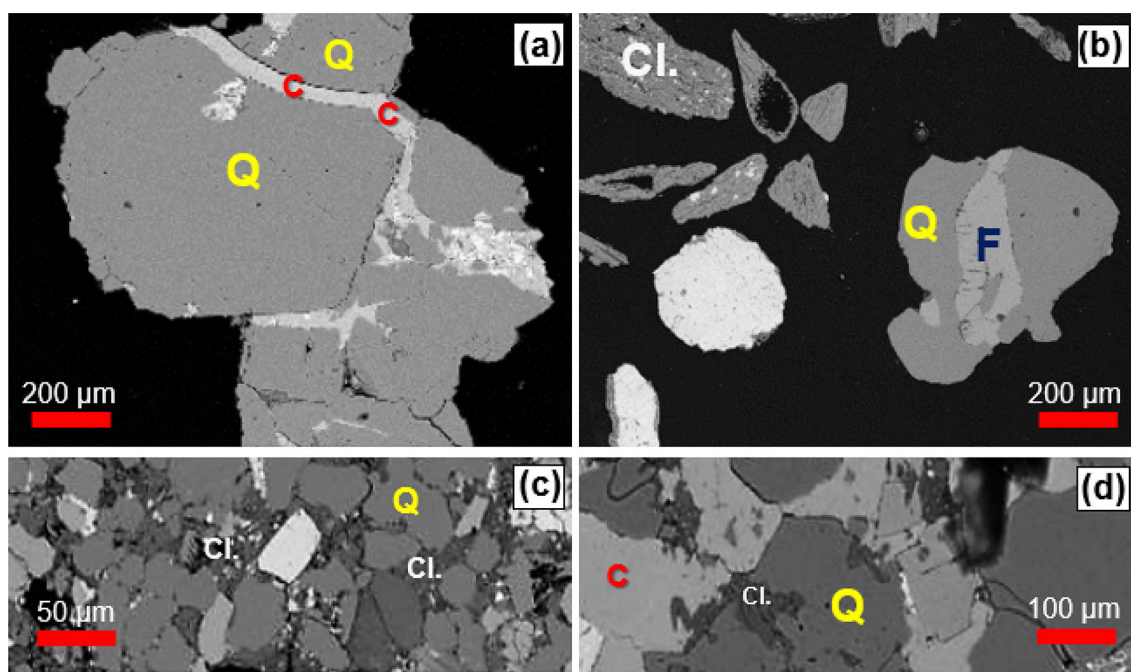* 1 mD (millidarcy) = 0.986923* 10^{-15} m^2

Figure 11. Thin section analyses of the Upper Miocene reservoir sandstones from Well-B using a Scanning Electron Microscope (SEM). (**a**) quartz grains with calcite cements at 2625 m (Zone 2C), (**b**) quartz with feldspar in the crack along with clay particles at 2660 m (Zone 2D), (**c**) grain supported texture at 2690 m (Zone 2D), (**d**) matrix-supported quartz grains with clay and calcite in pore spaces at 2694 m (Zone 2D). Q = quartz, F = Feldspar, C = Calcite, Cl. = Clay.
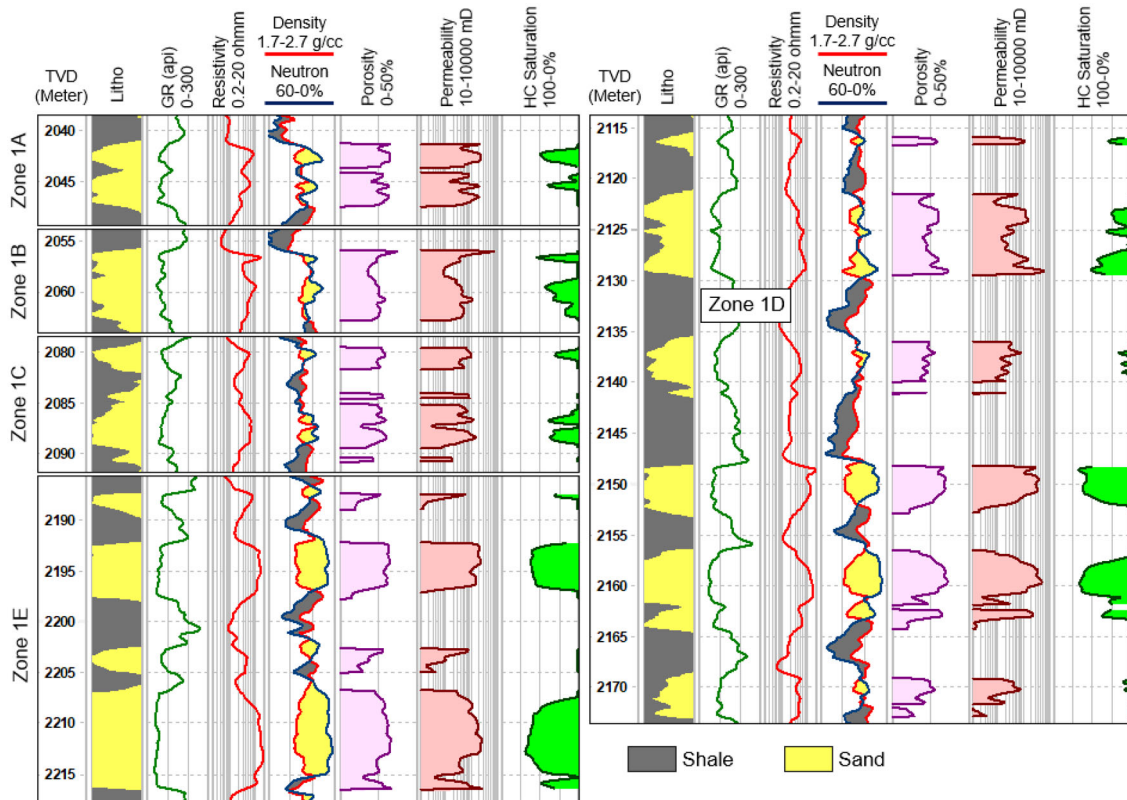
Figure 12. Log-based petrophysical evaluation of the Upper Miocene reservoir sandstones of Zone 1 from Well-B.

pipe in the Well-A. The minimum mud weight must be kept above 10.2 ppg while drilling the Upper Miocene section to ensure a stable wellbore.

DISCUSSION

Petroleum Geology of the Study Area and Implications for Hydrocarbon Exploration

Generally, rift basins continue to create both open marine and restricted settings that are favorable to source rock accumulation (Al Sharhan, 2003; Radwan et al., 2021a, 2021b). The mean sedimentary thickness of the Albert Basin is likely to be in excess of 5000 m, and it is composed of different lithologies, which make it a good target for hydrocarbon exploration (Lirong et al., 2004). Numerous oil seeps can be found in the basin, indicating the presence of a petroleum system (Fig. 1b) (Lirong et al., 2004). The analyses of these oil seep samples demonstrated that the oil was generated from two different source

rocks, which probably belong to the Cretaceous or Tertiary formations (Cheng et al., 2002; Lirong et al., 2004). The aforementioned results confirmed the richness of the overall petroleum system element within the Albert Basin. The overall petroleum system elements of the studied area are discussed below, and tentative events' are summarized in Table 5.

Source Rock

From a regional study of the Semliki Basin (Blocks 3B, 3C, and 3D), Lukaye et al. (2016) indicated an organic-rich oil-prone clastic source rock with possibility of good oil generation potential and they inferred the Semliki Basin as a good prospect for hydrocarbon plays with both structural and stratigraphic trapping. A NW–SE cross section of the studied field is presented in Figure 17. The presence of Type I/II good oil-prone source rock quality with 2–3 wt% TOC was established from this
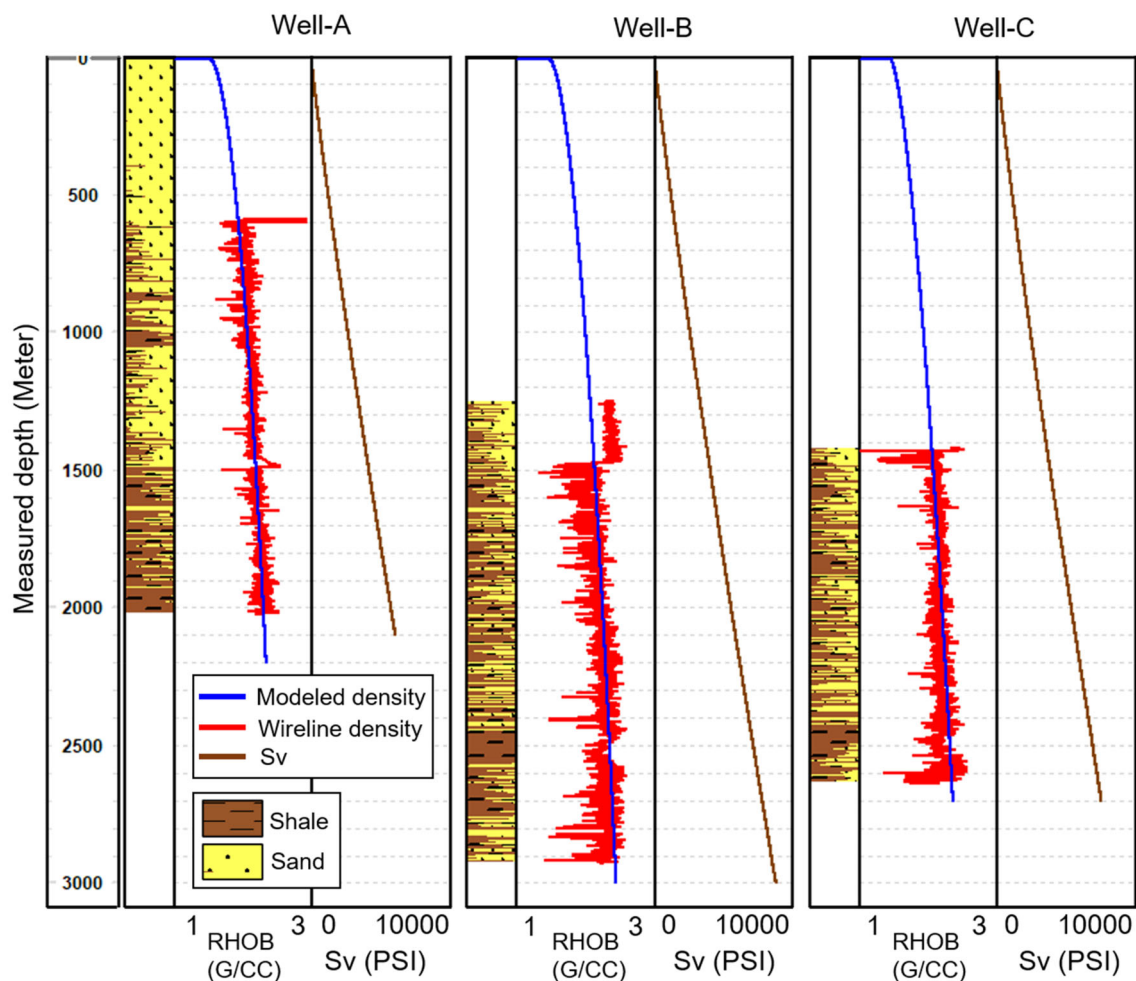
Figure 13. Modeling pseudo-density profile and vertical stress (S_v) magnitude in the three vertical exploratory wells drilled in the study area. Modeled density profile (blue) follows the trend of the wireline bulk-density log (red).

study. Based on the geochemical results presented in this work, Miocene shales of the Kakara–Kasande Formations are of early catagenetic maturity and define the source rock element of the regional petroleum system with the more mature deeper Miocene shales (> 3000 m) possibly being in the oil window. Subsurface temperature data acquired during logging runs indicate a present-day geothermal gradient of 35 °C/km and a bottom hole temperature of 120 °C (2500 m). The petroleum generation, which is both temperature and time dependent, generally occurs over the temperature range 100–150 °C for labile kerogen. The present-day bottom hole temperature might suggest a higher maturity level than that measured (R_o 0.5%, SCI 5). However, this is reconciled by taking into consid-

eration the time dependency of maturation, in which oil generation thresholds are generally deeper and occur at higher temperatures for young basins, as is the case for the studied well. An alternative explanation for the relatively high subsurface temperature and low measured maturity level could be a recent increase in the heat flow and geothermal gradient, due to actively ongoing tectonism which is common in many prolific basins (Ganguli et al., 2018).

Hydrocarbon Generation, Migration and Pathways

Following the expulsion, the hydrocarbon migrated from the impermeable source rock formations to the early Upper Miocene Kasande and
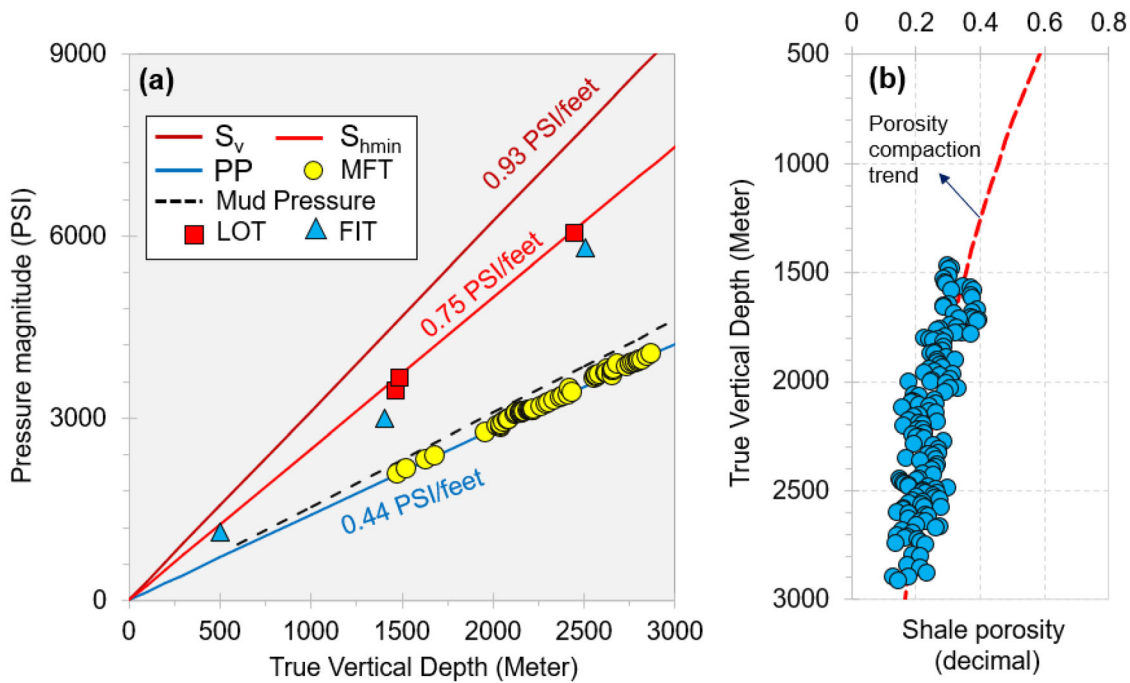
Figure 14. (a) Regional pore pressure, S_v and S_{hmin} magnitude plotted against vertical burial depth to interpret the subsurface pressure gradients. Calibration data (MFT, LOT, FIT, and drilling mud weight) from all the wells are plotted to validate the interpretation. (b) Shale porosity follows a compaction trend line with depth indicating hydrostatic shale porosity.

Kakara Formations' highly porous and permeable reservoirs. These are sandstones with intra-particle porosities that serve as the primary reservoirs for hydrocarbons. Generally, the rift structure is mainly dominated by faults, where the fault planes and associated fractures or micro-fractures represent favorable migration pathways (Hooper, 1991; Li et al., 2010; Radwan et al., 2021a, 2021b). Regional petroleum system modeling indicates that hydro-carbons were possibly generated from the lacustrine shales during the mid-Pliocene and migrated into the reservoirs during the late Pliocene (Simon et al., 2017). The study area is bounded by two major faults (Bunia and Tonya faults) along with the rift shoul-ders (Fig. 17). The boundary faults are on the basin's northwest and northeast sides, rendering it an asymmetrical half-graben. As well, the entire study area is affected by several faults controlling the en-tire structure and forming the overall structure. Thus, the migration of the generated hydrocarbon within the study area is most likely following the preferential petroleum migration pathways from the source to porous zones within the basin as well as dissipation along joints and permeability may also

contribute to lateral migration of hydrocarbon through the Miocene rocks.

Reservoir Rocks

The Albertine Graben, like the most Meso–Cenozoic basins in Africa, hosts many porous sandstones which act as main conventional reser-voirs. Previous studies conducted in the basin out-crops inferred two main sandstone reservoirs: (1) the Kisegi Formation (Middle Miocene), which is char-acterized by mixed sandstones and shales with minor silty facies deposited in a fluvial depositional envi-ronment; and (2) the Nyaburogo Formation (Upper Miocene to Middle Pliocene), which is characterized by sand/shale sequence deposited in delta plains and shoreface depositional environment. However, less porous and low permeability sandstones of the Nyaburogo Formation were recorded in the Semliki area (Lirong et al., 2004). In the study area, sand-stone reservoirs belong to the Kasande and Kakara Formations. The reservoir elements belong to the deltaic sandstones being deposited in a cyclic sedi-mentation during the Upper Miocene. These sand-
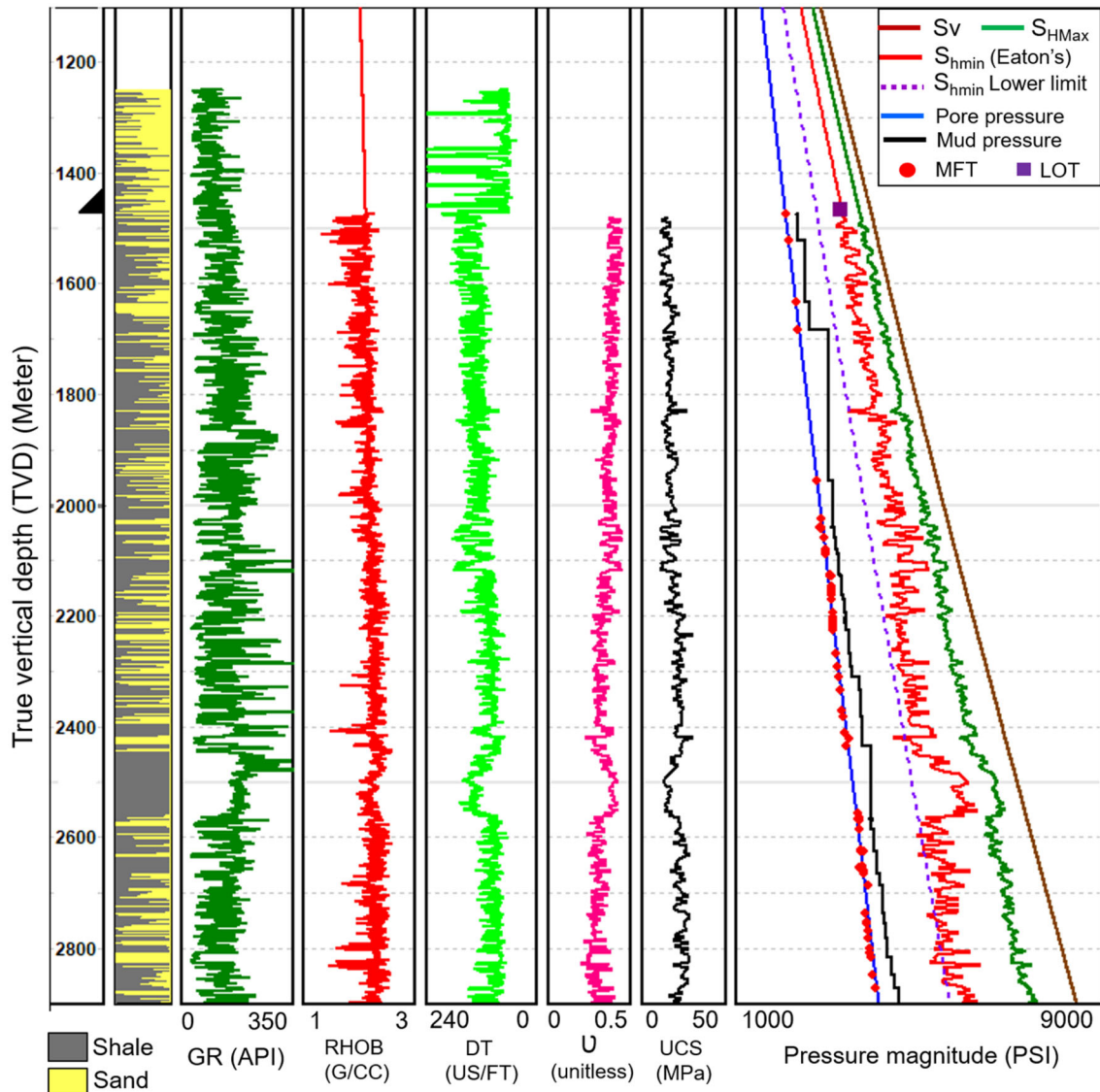
Figure 15. A comprehensive 1D mechanical earth model of the Well-B presenting the pore pressure, principal stress magnitudes along with the wireline logs, Poisson's ratio and rock strength (UCS). Note that the lower limit of S_{hmin} is modeled with frictional faulting theory, which corroborates with the Poisson's ratio based S_{hmin} estimate in the deeper section (> 2600 m TVD). Calibration data (MFT, LOT and drilling mud weight) are plotted to validate the results.

stone reservoir's gamma ray trends revealed box-car shapes which correspond to the prograding delta distributaries (Radwan, 2021a). These Miocene pay sands flowed at a 14,000 bopd rate in the nearby Kingfisher field which is the most successful oil discovery in the Albertine Graben, being situated to the northeastern part of our study area. The quartz arenites of our study area exhibit excellent storage and flow potential and possess a gas gradient of 0.17–0.24 psi/ft in two distinguishable zones of 206 m gross vertical thickness. Our wireline log-

based calculations estimated a reservoir porosity range of 19–32% with permeability varying between 100 and 5000 mD. These values correlate well with the nearby EA1 exploration area of the Lake Albert Basin, where Ongin (2013) inferred 15–40% porosity and 100–9000 mD permeability in the equivalent channel sandstone reservoirs from the core measurements.
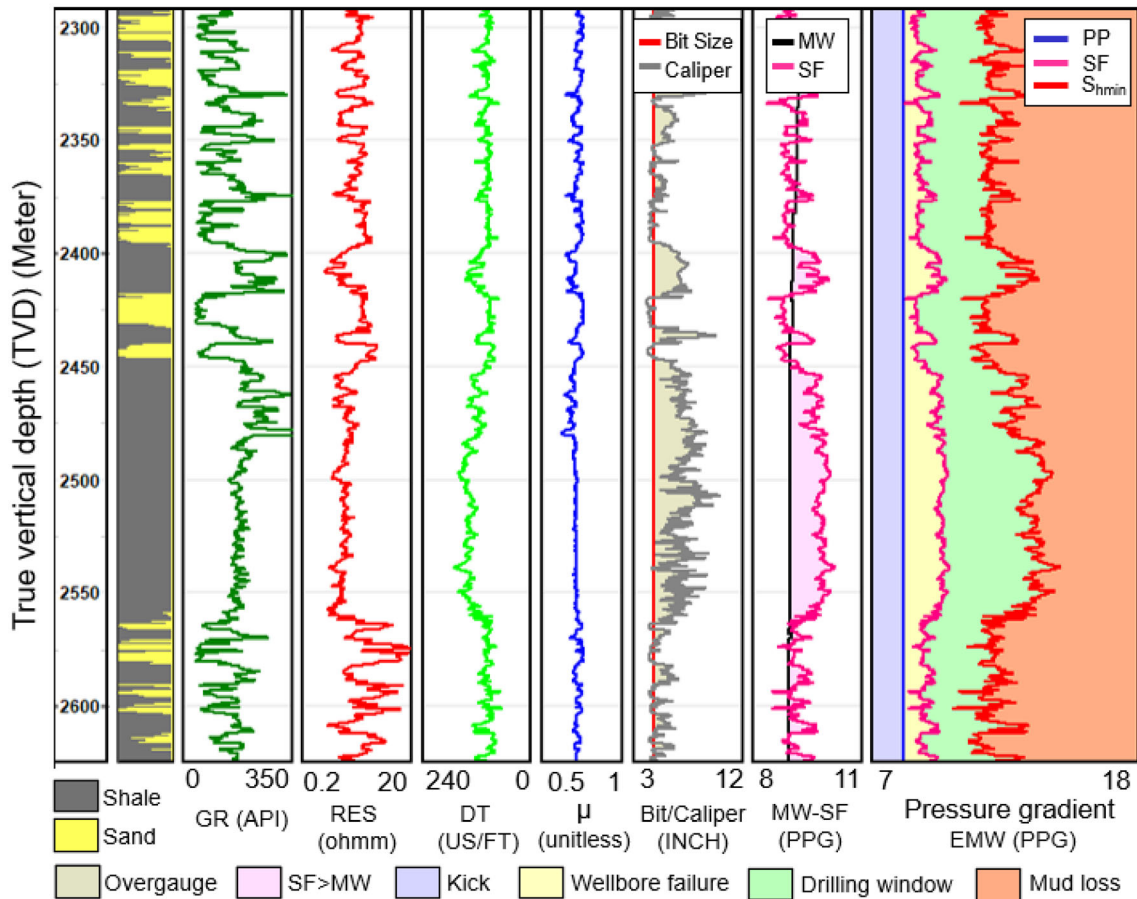
Figure 16. Wellbore stability model of Well-B, presenting the pore pressure, shear failure pressure (SF), and S_{hmin} gradient in terms of ppg unit (mud weight equivalent). Difference between the interpreted SF and used drilling mud weight (MW) corroborates with the bit size-caliper log difference, indicating overgauge well sections against shales. A safe mud window is presented along with the kick-failure-fluid loss gradients/limits (refer to the legends).

Table 5. Events' chart showing total petroleum system of the studied basin

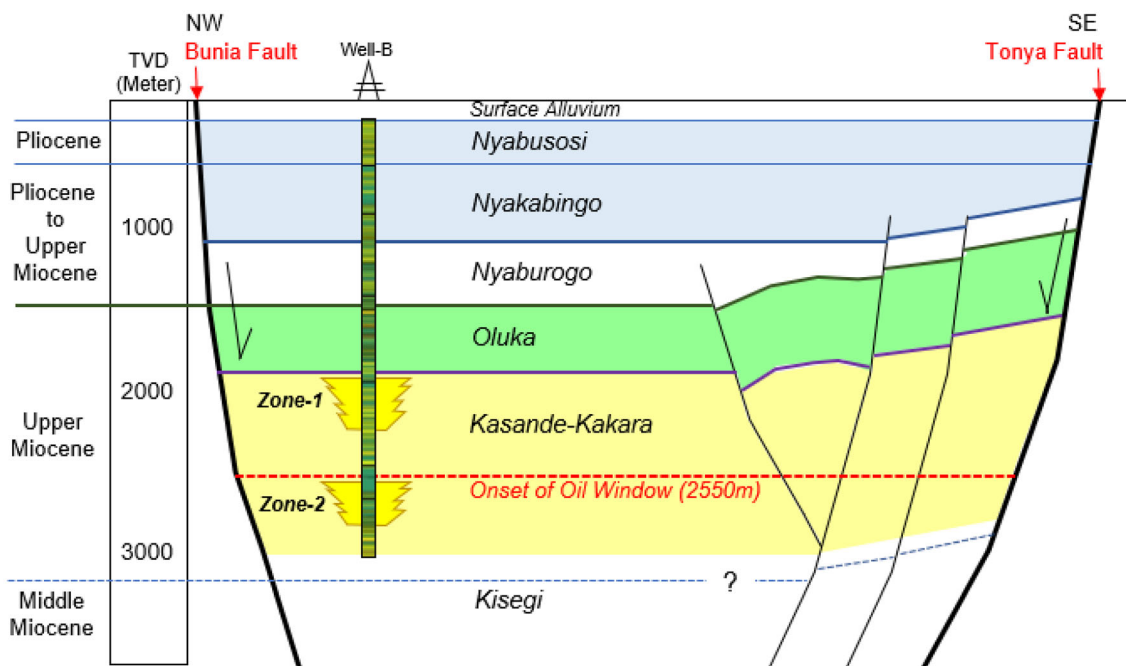| Age	Formation	Source rocks	Reservoir rocks	Seal Rocks	Overburden	Trap formation	Generation, migration and accumulation	Preservation
Pliocene	Nyabusosi							
Pliocene–Miocene	Nyakabingo							
Upper Miocene	Nyaburogo							
	Oluka							
	Kakara							
	Kasande							
Middle Miocene	Kisegi							

Figure 17. NW–SE cross-sectional visualization of the studied field through Well-B, along with the major basin bounding faults (Bunia and Tonya faults), reservoirs within the Upper Miocene Kasande–Kakara Formations (Zone 1 and 2) and the interpreted top of the oil window.

Hydrocarbon Entrapment and Seal Rocks

Petroliferous rift basins are characterized by a multi-entrapment system encompassing structural, stratigraphic, and combined entrapment systems (Demaison & Huizinga, 1991; Al Sharhan, 2003; Radwan et al., 2021a, 2021b). Based on the regional seismic interpretations, a variety of structural trapping mechanisms are reported in the forms of, among others, drape anticline, flower structures, and faulted blocks (Abeinomugisha & Kasande, 2012; Lirong et al., 2004; Simon et al., 2017). Lirong et al (2004) pointed to stratigraphic and combined traps, such as pinch-outs, and lithological changes within the basin. In addition, efficient migration is deciphered from the drilled wells and oil seepages. Matovu et al. (2015) worked on the shallow hazard assessment and interpreted various basement propagated faults in the northern part of the Lake Albert Basin. This observation along with the Bwamba fault (Semliki Basin) kinematics by Hollinsworth et al. (2018) possibly answers the extensive abundance of oil seeps along basin margin faults in and around the Lake Albert. Possible hydrocarbon accumulation may be located within any porous sandstone that has a connection down to deep hydrocarbon source rocks. The discovery of the gas-bearing sandstone reservoir zones in the Kasande and Kakara Formations in this study renewed the interest in subtle traps within the basin where these sandstone reservoirs are yet to be found in other unexplored areas of the Albertine Graben. The Miocene lacustrine shales provided the necessary vertical sealing to these reservoir rocks. The shales of the Kisegi Formation act as the basal seal, while the Oluka shales serve as the top seal. Furthermore, a lateral seal can be found in three different ways within the study basin: (1) juxtaposition, in which sandstone intervals are juxtaposed with impermeable shales as a consequence of the basin's structural settings; (2) facies change where the sandstone facies is laterally converted to impermeable lithology; and (3) lateral seal by the faults. The study area in the Albertine Graben offers a unique opportunity to look into the hydrocarbon generation potential in a young rift system.

Regional Geological Risk Analyses

Hydrocarbon exploration is mainly affected by the petroleum system elements within the sedimen-

tary basins. Therefore, the uncertainties regarding the distribution and thickness of the source rocks within the basin should be taken into consideration while exploring the potential hydrocarbon fields within the study area. As well, the stratigraphic continuities of the sandstone reservoirs should be taken into consideration as potential risk. High-resolution 3D seismic data will be helpful in delineating the lateral continuity of the potential reservoir facies. The seals may not have been well developed in some areas of the basin which can be followed by the effects of tectonics on the basin, and it can impact the faults' seal of hydrocarbon entrapments in structural traps.

Implications on Future Drilling

From a geomechanical perspective, the interpreted stress magnitudes ($S_v > S_{hmin}$) area is consistent with the regional extensional behavior. Regional horizontal stress orientation is influenced by the active rifting of EARS. The Tertiary stratigraphy is devoid of any overpressured interval, and the hydrostatically pressured interval excludes any potential drilling complexity owing to formation fluid influx. The high porosity and permeability nature of the reservoirs are indicative of excellent reservoir flow potential and, thus, hydraulic fracturing will not be required to ensure reservoir productivity. The shear failure gradient of the reservoir sandstones is observed to be lower than the pore pressure, and this implies that the production wells might not immediately face major solid production issues; however, the possibility is on the higher side considering the poor rock compressive strength. We recommend performing a core-based detailed rock strength measurement to optimize the completion strategy and avoid sanding issues in the long run. We recommend the use of a slotted liner in the completion design. Mechanical earth modeling was attempted to comment on the extensive wellbore failures in the Miocene shales which hindered the wireline data acquisition. Chuanliang et al. (2013) studied the Tertiary shales from the nearby Kingfisher oilfield and interpreted a shear failure gradient of 9.8–10.8 ppg, while the core-based experiment provided a shale uniaxial compressive strength of about 20 MPa. These results are in good agreement with the log-based rock strength (16–29 MPa UCS) and failure pressure magnitudes interpreted in the Upper Miocene shales in our study area. To address the caving and borehole wall collapse in the Upper Miocene

shale, this study inferred a minimum allowable drilling fluid pressure. Application of higher pump rate (still maintaining the equivalent circulating density below the lower limit of S_{hmin}) and high viscosity pills while drilling the Miocene sections can be useful to clean the wellbore if the cutting removal issue is observed.

CONCLUSIONS

With some impressive exploration success in the eastern and northern parts of the Lake Albert, several activities focused on the unexplored parts of the Albertine Graben. Here, we discussed the results from integrated geological analyses of a potential area in the Semliki Basin, situated at the southern tip of the Lake Albert, which has been the primary target of recent exploratory activities. This study characterized the source rock geochemical properties of the Upper Miocene shales of the Oluka and Kakara–Kasande Formations in the Semliki Basin. A Type I/II source rock with a fair TOC range was interpreted in the Miocene interval, which is presently at the early catagenic maturation stage. The source rock potential suggests the generation and expulsion of mixed oil and gas in suitable temperature and pressure conditions. The present study indicates an established petroleum system in the southern part of the Lake Albert; however, we suggest that future exploratory and appraisal wells should target the deeper Miocene intervals (> 3000 m), which will have more thermal maturity in the oil window. Wireline log-based evaluation indicates superior petrophysical characteristics within the gas-bearing sandstones. The presented mechanical earth modeling provides a confident estimate of formation pore pressure, vertical stress, minimum horizontal stress, and formation failure gradients. By analyzing the mechanical stuck-up encountered within the thick Upper Miocene shale interval, our wellbore stability study recommends a safe mud window for future drilling in the area to ensure borehole integrity. The results of this work will help the geoscience community working in the Albertine Graben to plan and execute the future exploratory and appraisal drilling campaign in a better and optimum manner.

ACKNOWLEDGMENTS

REFERENCES

Abdelghany, W. K., Radwan, A. E., Elkhawaga, M. A., Wood, D., Sen, S., & Kassem, A. A. (2021). Geomechanical modeling using the depth-of-damage approach to achieve successful underbalanced drilling in the Gulf of Suez Rift Basin. *Journal of Petroleum Science and Engineering, 202*, 108311.

Abeinomugisha, D., & Kasande, R. (2012). Tectonic control on hydrocarbon accumulation in the intracontinental Albertine Graben of the East African rift system. In D. Gao (Ed.), *Tectonics and sedimentation: Implications for petroleum systems: AAPG Memoir* (Vol. 100, pp. 209–228). American Association of Petroleum Geologists. https://doi.org/10.1306/13351554M1003539.

Agbasi, O. E., Sen, S., Inyang, N. J., & Etuk, S. E. (2021). Assessment of pore pressure, wellbore failure and reservoir stability in the Gabo field, Niger Delta, Nigeria—Implications for drilling and reservoir management. *Journal of African Earth Sciences, 173*, 104038.

Alsharhan, A. S. (2003). Petroleum geology and potential hydrocarbon plays in the Gulf of Suez rift basin, Egypt. *AAPG Bulletin, 87*(1), 143–180.

Baban, D. H., & Ahmed, S. M. (2014). Vitrinite reflectance as a tool for determining level of thermal maturity for the Upper Jurassic Naokelekan and Barsarin Formations in Sargelu location, Kurdistan Region, NE Iraq. *Arabian Journal of Geosciences, 7*, 2269–2277.

Baouche, R., Sen, S., Chaouchi, R., & Ganguli, S. S. (2021a). Modeling In-situ tectonic stress state and maximum horizontal stress azimuth in the Central Algerian Sahara—A geomechanical study from EL Agreb, El Gassi and Hassi Messaoud field. *Journal of Natural Gas Science and Engineering, 88*, 103831.

Baouche, R., Sen, S., Debiane, K., & Ganguli, S. S. (2020b). Integrated reservoir characterization of the Paleozoic and Mesozoic sandstones of the El Ouar field, Algeria. *Journal of Petroleum Science and Engineering, 194*, 107551.

Baouche, R., Sen, S., & Ganguli, S. S. (2020a). Pore pressure and in-situ stress magnitudes in the Bhiret Hammou hydrocarbon field, Berkine Basin, Algeria. *Journal of Africa Earth Sciences, 171*, 103945.

Baouche, R., Sen, S., Ganguli, S. S., & Boutaleb, K. (2021c). Petrophysical and geomechanical characterization of the Late Cretaceous limestone reservoirs from the Southeastern Constantine Basin, Algeria. *Interpretation, 9*(4), 1–36.

Baouche, R., Sen, S., Ganguli, S. S., & Feriel, H. A. (2021b). Petrophysical, geomechanical and depositional environment characterization of the Triassic TAGI reservoir from the Hassi Berkine South field, Berkine Basin, Southeastern Algeria. *Journal of Natural Gas Science and Engineering, 91*, 104002.

Barnard, P. C., Collins, A. G., & Cooper, B. S. (1981). Identification and distribution of kerogen facies in a source rock horizon—Examples from the North Sea Basin. In J. Brooks (Ed.), *Organic maturation studies and fossil fuel exploration* (pp. 271–282). Academic Press.

Calais, E., Ebinger, C., Hartndy, C., & Nocquet, J. M. (2006). Kinematics of the East African Rift from GPS and earthquake slip vector data. In G. Yirgu, C. J. Ebinger, & P. K. H. Macguire (Eds.), *The afar volcanic province within the East African Rift system* (Vol. 259, pp. 9–22). Geological Society London Special Publications.

Cassie, B., Sheen, C., & Burden, P. (2015). Discovering oil in Uganda: Opening the East African rift play. In *AAPG International Conference and Exhibition, Melbourne, Australia*, Sept 13–16. Search and Discovery Article #110224.

Cheng, D., Lirong, D., Jianjun, W., Rubondo, E. N. T., Kasande, R., Byakagaba, A., & Mugisha, F. (2002). Geochemical characteristics of shales and oil seepages in the Albertine Graben. *Geochimica (beijing), 31*(6), 532–538. (in Chinese with English abstract).

Chuanliang, Y., Jinger, D., Baohua, Y., & Jinxiang, L. (2013). Rock mechanical characteristics and wellbore stability in Kingfisher oilfield of Uganda. *SOCAR Proceedings*. https://doi.org/10.5510/OGP20130300164.

Cloke, I., Cowley, S., & Rindfuss, R. (2018). Hydrocarbon exploration history of Uganda. *GEOExPro, 15*(5).

Dellisanti, F., Pini, G. A., & Baudin, F. (2010). Use of Tmax as a thermal maturity indicator in orogenic successions and comparison with clay mineral evolution. *Clay Minerals, 45*(1), 115–130.

Delvaux, D., & Barth, A. (2010). African stress pattern from formal inversion of focal mechanism data. *Tectonophysics, 482*(1–4), 105–128.

Demaison, G., & Huizinga, B. J. (1991). Genetic classification of petroleum systems. *AAPG Bulletin, 75*(10), 1626–1643.

Dembicki, H., Jr. (2017). Chapter 3—Source rock evaluation. In H. Dembicki Jr. (Ed.), *Practical petroleum geochemistry for exploration and production* (pp. 61–133). Elsevier.

Eaton, B. A., & Eaton, T. L. (1997). Fracture gradient prediction for the new generation. *World Oil, 218*, 93–100.

Gagnevin, D., Tyrrell, S., Morton, A. C., Leather, J., Lee, N., Bordas-Le Floch, N., Frei, D., & Lukaye, J. (2017). Sand supply to the Lake Albert Basin (Uganda) during the Miocene–Pliocene: A multiproxy provenance approach. *Geochemistry, Geophysics, Geosystems, 18*, 2133–2148.

Ganguli, S. S., Vedanti, N., Pandey, O. P., & Dimri, V. P. (2018). Deep thermal regime, temperature induced over-pressured zone and implications for hydrocarbon potential in the Ankleshwar oil field, Cambay basin, India. *Journal of Asian Earth Sciences, 161*, 93–102.

Gholami, R., Moradzadeh, A., Rasouli, V., & Hanachi, J. (2014). Practical application of failure criteria in determining safe mud weight windows in drilling operations. *Journal of Rock Mechanics and Geotechnical Engineering., 6*(1), 13–25.

Hollinsworth, A. D., Koehn, D., Dempster, T. J., & Aanyu, K. (2018). Structural controls on the interaction between basin fluids and a rift flank: Constraints from the Bwamba Fault, East African Rift. *Journal of Structural Geology, 118*, 236–249.

Hooper, E. C. D. (1991). Fluid migration along growth faults in compacting sediments. *Journal of Petroleum Geology, 14*, 161–180.

Jakeman, B. L., & Cook, A. C. (1978). The dispersion of some optical properties of vitrinite. *Journal of Microscopy, 112*(2), 183–195.

Karner, G. D., Byamungu, B. R., Ebinger, C. J., Kampunzu, A. B., Mukasa, R. K., Nyakaana, J., Rubondo, E. N. T., & Upcott, N. M. (2000). Distribution of crustal extension and regional basin architecture of the Albertine rift system. *East Africa. Marine and Petroleum Geology, 17*(10), 1131–1150.

Karp, T., Scholz, C. A., & Mcglue, M. M. (2012). Structure and stratigraphy of the Lake Albert Rift, East Africa: Observations from seismic reflection and gravity data. In O. W. Baganz, Y. Bartov, K. M. Bohacs, & D. Nummedal (Eds.), *Lacustrine sandstone reservoirs and hydrocarbon systems* (p. 95). AAPG Memoir. https://doi.org/10.1306/13291394M9529 03.

Kassem, A. A., Sen, S., Radwan, A. E., Abdelghany, W. K., & Abioui, M. (2021). Effect of depletion and fluid injection in the Mesozoic and Paleozoic sandstone reservoirs of the October Oil Field, Central Gulf of Suez Basin: Implications on drilling, production and reservoir stability. *Natural Resources Research, 30*, 2587–2606.

Kibria, M. G., Das, S., Hu, Q., Basu, A. R., Hu, W., & Mandal, S. (2020). Thermal maturity evaluation using Raman spectroscopy for oil shale samples of USA: Comparisons with vitrinite reflectance and pyrolysis methods. *Petroleum Science, 17*, 567–581.

Koehn, D., Lindenfeld, M., Rümpker, G., Aanyu, K., Haines, S., Passchier, C. W., & Sachau, T. (2010). Active transsection faults in rift transfer zones: Evidence for complex stress fields and implications for crustal fragmentation processes in the western branch of the east African rift. *International Journal of Earth Sciences, 99*, 1633–1642.

Lang, J., Li, S., & Zhang, J. (2011). Wellbore stability modeling and real-time surveillance for deep water drilling to weak bedding planes and depleted reservoirs. In *SPE/IADC drilling conference and exhibition held in Amsterdam, The Netherlands*, March 1–3. SPE-139708-MS. https://doi.org/10.2118/139708-MS.

Leila, M., Sen, S., Abioui, M., & Moscariello, A. (2021). Investigation of pore pressure, in-situ stress state and borehole stability in the West and South Al-Khilala hydrocarbon fields, Nile Delta, Egypt. *Geomechanics and Geophysics for Geo-Energy and Geo-Resources, 7*, 56.

Li, S., Pang, X., Jin, Z., Li, M., Liu, K., Jiang, Z., Qiu, G., & Gao, Y. (2010). Molecular and isotopic evidence for mixed-source oils in subtle petroleum traps of the Dongying South Slope, Bohai Bay Basin. *Marine and Petroleum Geology, 27*(7), 1411–1423.

Lirong, D., Jianjun, W., Dingsheng, C., Xuefeng, R., Rubondo, E. N. T., Kasande, R., Byakagaba, A., & Mugisha, F. (2004). Geological conditions and petroleum exploration potential of the Albertine Graben of Uganda. *Acta Geologica Sinica, 78*(4), 1002–1010.

Lukaye, J., Worsley, D., Kiconco, L., Nabbanja, P., Abeinomugisha, D., Amusugut, C., Njabire, N., Nuwagaba, R., Mugisha, F., Ddungu, T., Sserubiri, T., & Sempala, V. (2016). Developing a coherent stratigraphic scheme of the Albertine Graben-East, Africa. *Journal of Earth Science and Engineering, 6*, 264–294.

Matovu, G. R., Kibirango, J., Bidgood, T., Businge, L., Cryan, J., & Dawson, K. (2015). Shallow geohazards assessment study for field development projects, Lake Albert Basin. In: International petroleum technology conference (IPTC), Doha, Qatar, Dec 6–9. IPTC-18412-MS. https://doi.org/10.2523/IPTC-18412-MS.

Min, G., & Hou, G. (2018). Geodynamics of the East African Rift System ~30 Ma ago: A stress field model. *Journal of Geodynamics, 117*, 1–11.

Morley, C. K. (2010). Stress re-orientation along zones of weak fabrics in rifts: An explanation for pure extension in 'oblique' rift segments? *Earth and Planetary Science Letters, 297*, 667–673.

Ongin, T. (2013). *Reservoir characterisation: Multi-scales Permeability data integration: Lake Albert Basin, Uganda.* MSc Thesis, Dept. of Earth Science and Engineering, Imperial College London.

Patra, S., Dirghangi, S. S., Rudra, A., Dutta, S., Ghosh, S., Varma, A. K., Shome, D., & Kalpana, M. S. (2018). Effects of thermal maturity on biomarker distributions in Gondwana colas from the Satpura and Damodar Valley Basins, India. *International Journal of Coal Geology, 196*, 63–81.

Pickford, M., Senut, B., & Hadoto, D. (1993). *Geology and palaeobiology of the Albertine Rift Valley, Uganda-Zaire. Vol. I: Geology* (Vol. 24, pp. 1–190). International Centre for Training and Exchanges in Geosciences Occasional Publications.

Radwan, A. E. (2021a). Modeling the depositional environment of the sandstone reservoir in the middle miocene sidri member, badri field, Gulf of Suez Basin, Egypt: Integration of gamma-ray log patterns and petrographic characteristics of lithology. *Natural Resources Research, 30*, 431–449.

Radwan, A. E. (2021b). Modeling pore pressure and fracture pressure using integrated well logging, drilling based interpretations and reservoir data in the Giant El Morgan oil Field, Gulf of Suez, Egypt. *Journal of African Earth Sciences, 178*, 104165.

Radwan, A. E., Abudeif, A. M., Attia, M. M., Elkhawaga, M. A., Abdelghany, W. K., & Kassem, A. A. (2020). Geopressure evaluation using integrated basin modelling, well-logging and reservoir data analysis in the northern part of the Badri oil field, Gulf of Suez, Egypt. *Journal of African Earth Sciences, 162*, 103743.

Radwan, A. E., Abudeif, A. M., Attia, M. M., & Mohammed, M. A. (2019). Pore and fracture pressure modeling using direct and indirect methods in Badri Field, Gulf of Suez, Egypt. *Journal of African Earth Sciences, 156*, 133–143.

Radwan, A. E., Rohais, S., & Chiarella, D. (2021a). Combined stratigraphic-structural play characterization in hydrocarbon exploration: A case study of Middle Miocene sandstones, Gulf of Suez basin, Egypt. *Journal of Asian Earth Sciences, 218*, 104686.

Radwan, A., & Sen, S. (2021a). Stress path analysis for characterization of in situ stress state and effect of reservoir depletion on present-day stress magnitudes: reservoir geomechanical modeling in the Gulf of Suez Rift Basin, Egypt. *Natural Resources Research, 30*, 463–478.

Radwan, A. E., & Sen, S. (2021b). Characterization of in-situ stresses and its implications for production and reservoir stability in the depleted El Morgan hydrocarbon field, Gulf of Suez Rift Basin, Egypt. *Journal of Structural Geology, 148*, 104355.

Radwan, A. E., Trippetta, F., Kassem, A. A., & Kania, M. (2021b). Multi-scale characterization of unconventional tight carbonate reservoir: Insights from October oil filed, Gulf of Suez rift basin, Egypt. *Journal of Petroleum Science and Engineering, 197*, 107968.

Riad, S., & El Etr, H. A. (1985). Bouguer anomalies and lithosphere-crustal thickness in Uganda. *Journal of Geodynamics, 3*(1–2), 169–186.

Roberts, E. M., Stevens, N. J., O'Connor, P. M., Dirks, P. H. G. M., Gottfried, M. D., Clyde, W. C., Armstrong, R. A., Kemp, A. I. S., & Hemming, S. (2012). Initiation of the western branch of the East African Rift coeval with the eastern branch. *Nature Geoscience, 5*, 289–294.

Rudra, A., Dutta, S., & Raju, S. V. (2017). The paleogene vegetation and petroleum system in the tropics: A biomarker approach. *Marine and Petroleum Geology, 86*, 38–51.

Saria, E., Calais, E., Stamps, D. S., Delvaux, D., & Hartnady, C. J. H. (2014). Present-day kinematics of the East African Rift. *Journal of Geophysical Research: Solid Earth, 119*(4), 3584–3600.

Schneider, S., Hornung, J., & Hinderer, M. (2016). Evolution of the western East African Rift system reflected in provenance changes of miocene to pleistocene synrift sediments (Albertine Rift, Uganda). *Sedimentary Geology, 343*, 190–205.

Simon, B., Guillocheau, F., Robin, Cé., Dauteuil, O., Nalpas, T., Pickford, M., Senut, B., Lays, P., Bourges, P., & Bez, M. (2017). Deformation and sedimentary evolution of the Lake Albert Rift (Uganda, East African Rift System). *Marine and Petroleum Geology, 86*, 17–37.

Stamps, D. S., Calais, E., Saria, E., Hartnady, C., Nocquet, J.-M., Ebinger, C. J., & Fernandes, R. M. (2008). A kinematic model for the East African Rift. *Geophysical Research Letters, 35*(5), L05304.

Stamps, D. S., Flesch, L. M., Calais, E., & Ghosh, A. (2014). Current kinematics and dynamics of Africa and the East African Rift System. *Journal of Geophysical Research Solid Earth, 119*(6), 5161–5186.

Tissot, B. P., Pelet, R., & Ungerer, P. H. (1987). Thermal history of sedimentary basins, maturation indices, and kinetics of oil and gas generation1. *AAPG Bulletin, 71*(12), 1445–1466.

Waples, D. W. (1985). Analytical techniques. In D. W. Waples (Ed.), *Geochemistry in petroleum exploration. Geological sciences series.* Springer. https://doi.org/10.1007/978-94-009-5436-6_7.

Wei, X., Lei, F., Xinye, Z., Penfegi, W., Xiaoli, Y., Xipu, Y., & Jun, L. (2017). Object-based 3D geomodel with multiple constraints for early Pliocene fan delta in the south of Lake Albert Basin, Uganda. *Journal of African Earth Sciences, 125*, 1–10.

Xu, W., Zhang, X., Shang, F., Fang, L., Liu, J., & Yang, X. (2018). An integrated quantitative approach for determination of net reservoir cutoffs: A case study of Q oil field, Lake Albert, Uganda. *Journal of African Earth Sciences, 145*, 261–266.

Yule, B., Roberts, S., Marshall, J. E. A., & Milton, J. A. (1998). Quantitative spore colour measurement using color image analysis. *Organic Geochemistry, 28*(3–4), 139–149.

Zhang, J. (2013). Borehole stability analysis accounting for anisotropies in drilling to weak bedding planes. *International Journal of Rock Mechanics and Mining Sciences, 60*, 160–170.

Zoback, M. D. (2007). *Reservoir geomechanics.* Stanford University.